Journal Title
XX(X):1–24

DOI: 10.1177/ToBeAssigned
www.sagepub.com/
SAGE

On the Motion/Stiffness Decoupling Property of Articulated Soft Robots with Application to Model-Free Torque Iterative Learning Control

Riccardo Mengacci[1], Franco Angelini[1,2], Manuel G. Catalano[2], Giorgio Grioli[2], Antonio Bicchi[1,2] and Manolo Garabini[1]

Abstract

This paper tackles the problem of controlling *articulated soft robots (ASRs)*, i.e., robots with either fixed or variable elasticity lumped at the joints. Classic control schemes rely on high-authority feedback actions, which have the drawback of altering the desired robot softness. The problem of accurate control of ASRs, without altering their inherent stiffness, is particularly challenging because of their complex and hard-to-model nonlinear dynamics. Leveraging a learned anticipatory action, Iterative Learning Control (ILC) strategies do not suffer from these issues. Recently, ILC was adopted to perform position control of ASRs. However, the limitation of position-based ILC in controlling variable stiffness robots is that whenever the robot stiffness profile is changed, a different input action has to be learned. Our first contribution is to identify a wide class of ASRs, whose motion and stiffness adjusting dynamics can be proved to be decoupled. This class is described by two properties that we define: strong elastic coupling - relative to motors and links of the system, and their connections - and homogeneity - relative to the characteristics of the motors. Furthermore, we design a torque-based ILC scheme that, starting from a rough estimation of the system parameters, refines the torque needed for the joint positions tracking. The resulting control scheme requires minimum knowledge of the system. Experiments on variable stiffness robots prove that the method effectively generalizes the iterative procedure w.r.t. the desired stiffness profile and allows good tracking performance. Finally, potential restrictions of the method, e.g., caused by friction phenomena, are discussed.

Keywords

Variable Stiffness Actuator, Soft Robotics, Iterative Learning Control, Torque Control.

1 Introduction

Recent years have seen a growing interest in the design of robots whose mechanical structure is intentionally realized with compliant elements, i.e., *soft robots*. These robots are attracting wide attention because of the many interesting features, e.g. the possibility to perform cyclic motions and high dynamic tasks (Braun et al. 2012), to exploit natural dynamics (Vanderborght et al. 2006) and to allow a safe interaction with uncertain environments (Albu-Schaffer et al. 2008), (Bicchi and Tonietti 2004). Furthermore, these robots are typically divided in *continuum* and *articulated* soft robots (Della Santina et al. 2020), which can be considered as the counterparts of invertebrate and vertebrate animals, respectively. In this paper, we focus on articulated soft robots (ASRs), whose structure is composed of rigid parts (with a structural role similar to bones) and compliant joints (reproducing the visco-elastic behavior of muscles, tendons and ligaments). Compliant elements in articulated soft robots can have fixed elasticity as in *Series Elastic Actuators (SEAs)* (Pratt and Williamson 1995) or a variable elasticity. The latter are known as *Variable Stiffness Actuators (VSAs)* (Vanderborght et al. 2013).

The main benefit of using VSAs is the possibility to vary the compliant behavior of the output link according to the desired task. There are several solutions, detailed in Vanderborght et al. (2013), that allow for the variation of compliance, e.g. the pre-loading of springs or the modification of the transmission ratio from the spring(s) to the motor output link. One of the main challenges in controlling VSA powered robots is to obtain an accurate trajectory tracking without losing the prescribed compliant behavior.

In the last decade, several works have been published to study the control of these actuators. Among them, we can find methods based on *PD with Gravity compensation* (De Luca and Flacco 2011), *Feedback Linearization* (Buondonno and De Luca 2016), (De Luca et al. 2009) and *BackStepping* (Petit et al. 2015). More recently, the authors in Keppler et al. (2018) proposed a control strategy purposefully designed to achieve motion tracking while preserving the elastic structure of the system. All these strategies rely on the dynamic model and require the knowledge of the torque-deflection characteristic of the

[1]Centro di Ricerca Enrico Piaggio, Universita' di Pisa, Largo Lucio Lazzarino 1, 56126 Pisa, Italy
[2] Soft Robotics for Human Cooperation and Rehabilitation, Istituto Italiano di Tecnologia, via Morego, 30, 16163 Genova, Italy
Email: riccardo.mengacci@gmail.com

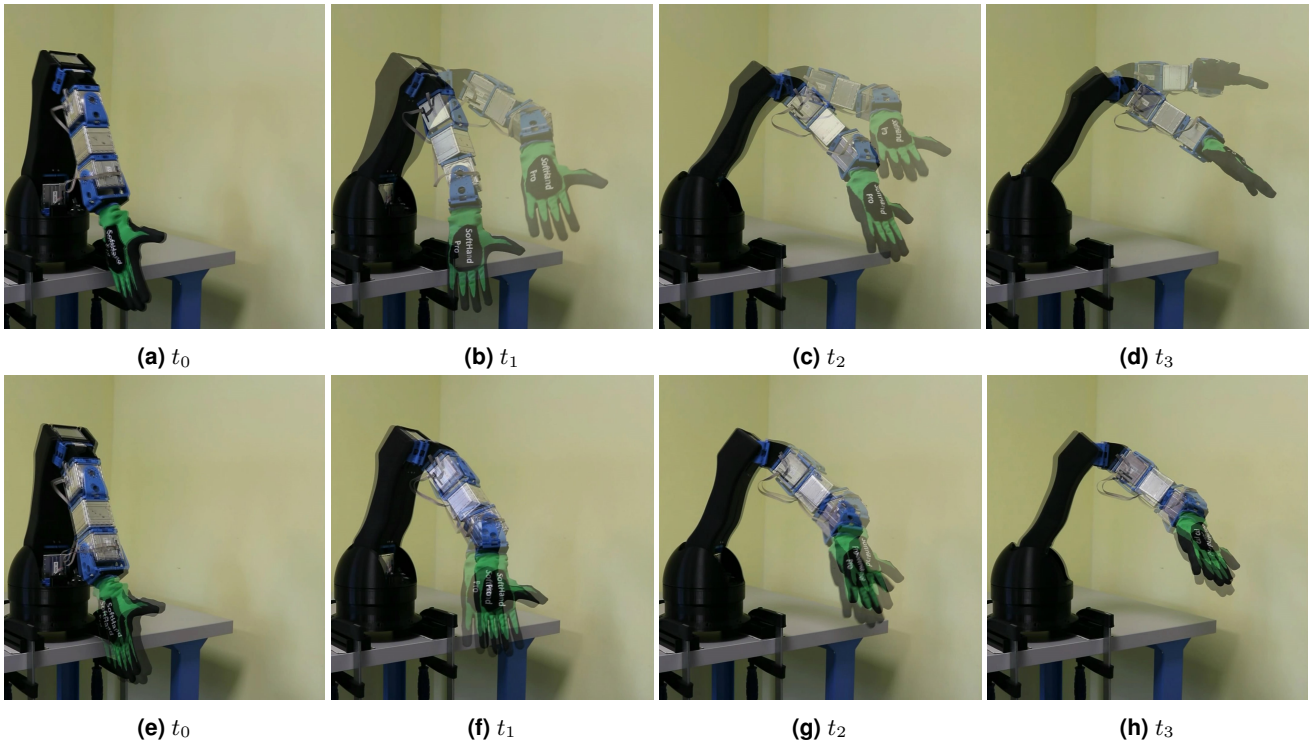

(a) t_0 **(b)** t_1 **(c)** t_2 **(d)** t_3

(e) t_0 **(f)** t_1 **(g)** t_2 **(h)** t_3

Figure 1. Frames of the trajectory tracking time sequence in case of pILC (a-d) and tILC (e-h) methods. The first sequence (a-d) shows that, with the same position control action and two different values of the stiffness regulation parameter (from soft to stiff), the resulting robot trajectory presents non negligible variation. Differently, in the second sequence (e-h), given the same torque control action and two different stiffness values, the robot position tracking is much less alterated. The 6-DOF manipulator used for the experiments and shown in picture is equipped with VSA-Cube actuators (Catalano et al. 2011) and a Pisa/IIT SoftHand (Della Santina et al. 2017b)

elastic elements of the system. This relationship maps the deflection of the output link from its equilibrium point to the variation of the external load applied. The lack of complete knowledge of this model requires the implementation of estimation or identification methods. To solve this issue, Flacco and De Luca (2011) proposed a parametric identification method, which requires an accurate model of the actuators, while in Flacco and De Luca (2014) the same authors presented a signal-based approach to estimate the stiffness. Most of the control laws from De Luca and Flacco (2011) to Keppler et al. (2018) use *FeedBack (FB)* terms on the variable to be controlled. As discussed in Della Santina et al. (2017a), closing the control loop over the link position can considerably alter the dynamic behavior of the system, up to the point of removing the benefits of intrinsic compliance. According to Della Santina et al. (2017a), the use of *FeedForward (FF)* control actions are preferable to preserve the natural behavior of the robot. Thus, balancing a predominant FF term and a low-gain FB component can lead to an accurate trajectory tracking while preserving the designed dynamics of the robot.

Following this idea, in Angelini et al. (2018) an *Iterative Learning Control (ILC)* scheme was recently proposed to generate a FF control action for articulated soft robots in which the position motor references, needed to track a desired link trajectory with a defined compliant profile, are iteratively refined. For this reason, we refer to this method as a *position-based ILC (pILC)*. The advantages of the iterative learning approach are: model-independence, softness preservation and a reduced set of gains to tune. Although the pILC scheme in Angelini et al. (2018) showed good results, it presents an undesirable coupling between motion control action and stiffness. This implies that, to execute a trajectory for which the control action was previously learned with a different stiffness profile, a new learning process is required, Fig. 1 (a-d).

To improve the applicability of this approach, exploiting the ILC benefits, we propose a control strategy, named *torque-based ILC (tILC)*, in which this undesired coupling effect is eliminated by generating a torque-based control action. This strategy derives from a twofold contribution: i) we introduce two properties that an ASR can have: strong elastic coupling and homogeneity. Then, we prove that the dynamics of a strong elastically coupled and homogeneous ASR can be decoupled in two parts: a flexible robot dynamics and an adjusting dynamics. Each part can be controlled by a separate torque component; ii) we adopt an ILC approach to design the first torque component, mostly in FF, useful to perform trajectory tracking, while the other is used to control the compliant behavior in FB. As a result of the motion/stiffness decoupling, which requires minimum knowledge of the system, and the use of an iterative approach, the control strategy proposed is model-free, meaning that it does not require any knowledge of the dynamics parameters.

The proposed control scheme shows good results in terms of trajectory tracking performance, and as well, it allows to independently vary the stiffness of the joints without affecting the tracking performance, Fig. 1 (e-h). This means that the limitation posed by the pILC

is overcome, i.e. that the control action learned with the tILC method can be reused with different compliant behavior, reducing the iterations needed to regain tracking performances. Experimental results show that the number of iterations and the tracking error achieved at convergence, are strongly related to the amount of friction affecting the system: the main limitation for the control strategy proposed. Furthermore, the method can be applied to most of the variable joint stiffness structures proposed in the literature.

As an additional result, the proposed approach allows us to fully exploit the compliant nature of the robot when performing tasks in which, even undesired, interactions may be involved. Following the method we propose, the learning process can be safely and robustly performed with the robot controlled with a low stiffness profile. Once the learning process is completed, the robot stiffness can be changed to properly execute the task. In this regard, we discuss one practical example at the end of the experimental part.

After recalling the dynamic model of VSAs systems, Section 2 defines the treated problem by introducing the desired control requirements. In Section 3 a brief review of the control strategies in the State of the Art (S.o.A.) is reported, discussing their advantages and limitations. The proposed solution is introduced and analyzed in Section 4. Section 5 presents a set of experiments where the effectiveness of the method, compared also with S.o.A. techniques, is proved on articulated soft systems (Fig. 1 and Fig. 5). Finally, conclusions are drawn in Section 6.

2 Problem definition

2.1 Dynamic model

We here consider the dynamic model of an n-DOFs robot with lumped elasticity at the joints proposed in Albu-Schäffer and Bicchi (2016). This formulation assumes a negligible inertia coupling between motors and links and gravity potential energy dominated by the links. Then, the dynamic equations can be written as

$$\begin{cases} M(q)\ddot{q} + C(q,\dot{q})\dot{q} + G(q) + \dfrac{\partial V(q,\theta)^T}{\partial q} = \tau_{\text{ext}}, & (1) \\ J\ddot{\theta} + D\dot{\theta} + \dfrac{\partial V(q,\theta)^T}{\partial \theta} = \tau_{\text{m}}, & (2) \end{cases}$$

where $q \in \mathbb{R}^n$ are the link positions; $\theta \in \mathbb{R}^m$ are the motor positions; $M(q)$ and $C(q,\dot{q})$ are inertia and Coriolis, centrifugal and frictional terms, respectively, and $G(q)$ is the gravitational vector of the system. Hereinafter, the dependency of $M(q)$, $C(q,\dot{q})$ and $G(q)$ from the state variables $q, \dot{q}$ is omitted for the sake of clarity. J, D are inertia and damping constant diagonal matrices of the motors; $V(q,\theta)$ is the elastic potential; τ_{m} are the motor torques and τ_{ext} is the external torque (if present). Furthermore, we consider the ideal case in which the dissipative actions acting on the link side equation (1) are negligible or constant. We will discuss the implication of the presence of non-negligible and variable dissipative actions, e.g., friction phenomena, in Section 4.3.

2.2 The control problem

One of the main purposes of a generic robotic control scheme is trajectory tracking. In the case of compliant actuators, e.g., variable stiffness actuators, regulation of the link position results in a non-trivial problem due to the elastic connection between motors and links. Indeed, the elastic mechanism is often nonlinear and hard-to-model. Furthermore, for VSA systems, the possibility to vary the stiffness during the task represents a key property, useful e.g., to exploit the intrinsic compliant behavior. The stiffness variation should be performed independently from the trajectory tracking and the control action should not alter it, e.g., in case of FB strategies, as discussed in Della Santina et al. (2017a).

Therefore, the problem addressed in this work is to define a control strategy that achieves the following goals:

- decoupling of the motion control from the stiffness control;
- accurate tracking of the desired link position trajectory;
- independence from the torque/deflection model;
- preservation of the stiffness behavior;
- independence from the robot dynamic model.

3 State of the Art

This section briefly describes the control techniques proposed in the last decade for compliant actuators. Their main characteristics and limitations will be reported.

For ASRs equipped with compliant actuators in the specific class of agonistic-antagonistic (A-A) VSAs with $m = 2n$, i.e., where there are two motors associated with each link of the system, it is convenient to define the elastic deflection as the difference between link and motor position vectors, i.e., $\phi_i \triangleq q - \theta_i$, with $i = 1, 2$ number of the motor. Then, following De Luca et al. (2009), it can be observed that $V(q,\theta) = \sum_i V(\phi_i)$ from which (1) and (2) can be rewritten as follow

$$\begin{cases} M\ddot{q} + C\dot{q} + G + \tau_{\text{e}_1}(\phi_1) + \tau_{\text{e}_2}(\phi_2) = \tau_{\text{ext}} \\ J_1\ddot{\theta}_1 + D_1\dot{\theta}_1 - \tau_{\text{e}_1}(\phi_1) = \tau_1 \\ J_2\ddot{\theta}_2 + D_2\dot{\theta}_2 - \tau_{\text{e}_2}(\phi_2) = \tau_2 \end{cases}, \quad (3)$$

where J_i, D_i are inertia and damping constant matrices of the motors i and $\tau_{\text{e}_i} = \frac{\partial V(\phi_i)^T}{\partial \phi_i}$, for $i = 1, 2$. Referring to (3), the torque control strategy based on the *feedback linearization* approach, proposed in De Luca et al. (2009), considers τ_1 and τ_2 as control inputs of the actuators. As outputs of interest, the control scheme takes the link positions q and the link stiffnesses $\sigma = [\sigma_1 \ \dots \ \sigma_n]^T$ (each element defined as $\sigma_i = \frac{\partial \tau_{\text{e}_i}}{\partial q_i}$). Differentiating four times q and two times σ the following nonlinear torque control law holds

$$\begin{bmatrix} \tau_1 \\ \tau_2 \end{bmatrix} = A^{-1}(x)\left(\begin{bmatrix} v_1 \\ v_2 \end{bmatrix} - b(x) \right), \quad (4)$$

with $x = (\theta_1, \theta_2, q, \dot{\theta}_1, \dot{\theta}_2, \dot{q})^T$ state of the new system, $A(x)$ decoupling matrix (defined in De Luca et al. (2009)), assumed non-singular, and $b(x)$ vector of terms depending on x. The desired link positions $\hat{q}$ and the desired stiffnesses

$\hat{\sigma}$ can be tracked by choosing

$$\begin{aligned} v_1 &= \hat{q}^{[4]} + k_{\mathrm{q},3} e_{\mathrm{q}}^{[3]} + k_{\mathrm{q},2} \ddot{e}_{\mathrm{q}} + k_{\mathrm{q},1} \dot{e}_q + k_{\mathrm{q},0} e_{\mathrm{q}}, \\ v_2 &= \dddot{\hat{\sigma}} + k_{\sigma,1} \dot{e}_\sigma + k_{\sigma,0} e_\sigma, \end{aligned} \tag{5}$$

where $e_{\mathrm{q}} = \hat{q} - q$ and $e_\sigma = \hat{\sigma} - \sigma$, are the link position and stiffness errors with their derivatives, up to the third order (i.e., superscript $^{[3]}$), $\hat{q}^{[4]}$ is the fourth derivative of the desired link positions and $k_{\mathrm{q},i}, \forall i = 0 \dots 3$ and $k_{\sigma,j}, \forall j = 0, 1$ are the control gains.

More recently Keppler et al. (2018) propose a control strategy, named *elastic structure preserving (ESP)*, suitable to drive variable stiffness actuators with either A-A design or with adjusting stiffness mechanisms, i.e., where there is a motor specifically designed to vary the compliance. The basic idea in Keppler et al. (2018) is to introduce new coordinates $(\tilde{q}, \eta)$ that reflect the desired behavior of the link dynamics. Then, based on these new variables, it is possible to design a specific control input to regulate (or to track) a desired trajectory at the link with a desired damped behavior. In the following, we show a sketch of the method, the reader can refer to Keppler et al. (2018) for a detailed description. The method consists in imposing a desired dynamics written as

$$M(\tilde{q})\ddot{\tilde{q}} + C(\tilde{q}, \dot{\tilde{q}})\dot{\tilde{q}} + D_{\mathrm{q}}\dot{\tilde{q}} + \tau_{\mathrm{e}}(\tilde{q}, \eta) = \tau_{\mathrm{ext}}, \tag{6}$$

with D_{q} damping matrix satisfying specific conditions (see the reference paper), $\tilde{q} = q - \hat{q}$ tracking error coordinate and where $\tau_{\mathrm{e}}(\tilde{q}, \eta)$ is the resulting elastic torque function at the link evaluated in the new coordinates, i.e., $\tau_{\mathrm{e}}(\tilde{q}, \eta) = \frac{\partial V(\tilde{q}, \eta)^T}{\partial \tilde{q}}$. Then, equating (1) with (6), the new motor coordinate η can be computed by solving the follows

$$\tau_{\mathrm{e}}(\tilde{q}, \eta) = \tau_{\mathrm{e}}(q, \theta) + n(\tilde{q}, \dot{\tilde{q}}), \tag{7}$$

where $n(\tilde{q}, \dot{\tilde{q}})$ collects all the remaining terms. Note that (7) should be solved numerically (except for special cases). Finally, the control input is designed as

$$\begin{aligned} \tau_{\mathrm{m}} =& \tau_{\mathrm{e}}(q, \theta) + J(\dot{A}\dot{\eta} + \dot{\alpha}) + \\ & - JAJ^{-1}\left(\tau_{\mathrm{e}}(\tilde{q}, \eta) + K_{\mathrm{P}}\eta + K_{\mathrm{D}}\dot{\eta}\right) \end{aligned} \tag{8}$$

where J is the motor inertia matrix, $K_{\mathrm{P}}, K_{\mathrm{D}}$ are PD control gains and A, α are terms defined in Keppler et al. (2018).

For a more general class of compliant actuators, e.g., where there may be more than two motors per link, or even motors connected to multiple links, under conditions C.2 and C.3 in Braun et al. (2013), i.e., high gear-box reduction and high low-level position gains, it is possible to control directly the motors equilibrium position ($\theta_{\mathrm{r}} \in \mathbb{R}^n$). Then, other parameters $(m - n)$ can be defined in order to regulate additional free degrees of the system, e.g., to adjust the compliant behavior. In this last case, the free degree is represented by the stiffness regulation parameter (s.r.p.)* $\theta_{\mathrm{s}} \in \mathbb{R}^{(m-n)}$. Thus, given a specific θ_{s} and controlling through θ_{r} it is possible to track the link position by using the *inverse dynamic* approach (Braun et al. 2013). Indeed, for this control strategy, the system dynamics is

$$M\ddot{q} + C\dot{q} + G + \tau_{\mathrm{e}}(q, \theta_{\mathrm{r}}, \theta_{\mathrm{s}}) = \tau_{\mathrm{ext}}, \tag{9}$$

where τ_{e} is the overall elastic torque at the output link. From the link dynamic equation (9) the desired equilibrium position, needed to reach the desired link position, can be computed as

$$\hat{\theta}_{\mathrm{r}} = \hat{q} - \tau_{\mathrm{e}}^{-1}(\tau_{\mathrm{ext}} - M\ddot{\hat{q}} - C\dot{\hat{q}} - G). \tag{10}$$

The s.r.p. θ_{s} is used to evaluate τ_{e}^{-1}†.

Alternatively, to learn the control action needed to track the desired link trajectory, iterative approaches can be used. Following this idea, a position-based ILC (pILC) algorithm is proposed in Angelini et al. (2018). In the latter work the equilibrium position control input is computed in each iteration $k \in \mathbb{N}^+$ as

$$\theta_{\mathrm{r}}^k = \underbrace{\theta_{\mathrm{r}}^{k-1} + \theta_{\mathrm{UP}}^k}_{\theta_{\mathrm{FF}}^k} + \theta_{\mathrm{FB}}^k, \tag{11}$$

starting from an initial guess θ_{r}^0. θ_{FB}^k represents a feedback component added to improve the controller action. The stiffness of the system is imposed by choosing θ_{s}.

The aforementioned control strategies introduce the following drawbacks:

i) need for the system model (i.e., deflection function τ_{e} and dynamic matrices M, C, G),
ii) alteration of dynamic properties of the system,
iii) coupling between motion control and stiffness control.

More in detail, the *feedback linearization* approach allows to control either link position and link stiffness, decoupling the two control inputs. However, a drawback of the method is that it assumes that the inverse of the decoupling matrix, i.e., $\exists\ A^{-1}(x)$, exists. This method, as the *elastic structure preserving* control, requires also smooth reference trajectories. Moreover, the *feedback linearization* approach, the *elastic structure preserving* control and the *inverse dynamic* solution depend on both the model of the system and the model of the stiffness mechanism (i). Lastly, some of the aforementioned strategies may produce control laws that compromise the mechanical behavior of the system (ii).

On the other hand, the control strategy based on iterative learning is model-independent and preserves the stiffness behavior, as proved in Angelini et al. (2018). Thus, pILC overcomes the points (i) and (ii). However, the control action learned through iterations depends on a specific stiffness regulation parameter θ_{s}. This means that varying θ_{s} leads to the need for a new learning phase to recover from tracking performance loss (Fig. 1 (a-d)). For this technique, point (iii) represents an unsolved problem.

4 Control Design

In this section, we first define some properties of the elastic system in (1) and (2) and some assumptions from which it is possible to decouple the dynamics into two separate parts: a flexible joint robot dynamics and an adjusting dynamics. Then, we propose the torque-based ILC law that fulfills

*The equilibrium position and the s.r.p. are always given as functions of the motor positions. For instance for the VSA-Cube in Fig. 2b (bottom) these consist in the semi-sum and semi-difference of the motor positions (Della Santina et al. 2017b).

†To algebraically solve (10), the elastic torque function τ_{e} is supposed to be invertible. If this is not the case, then numerical methods should be adopted.

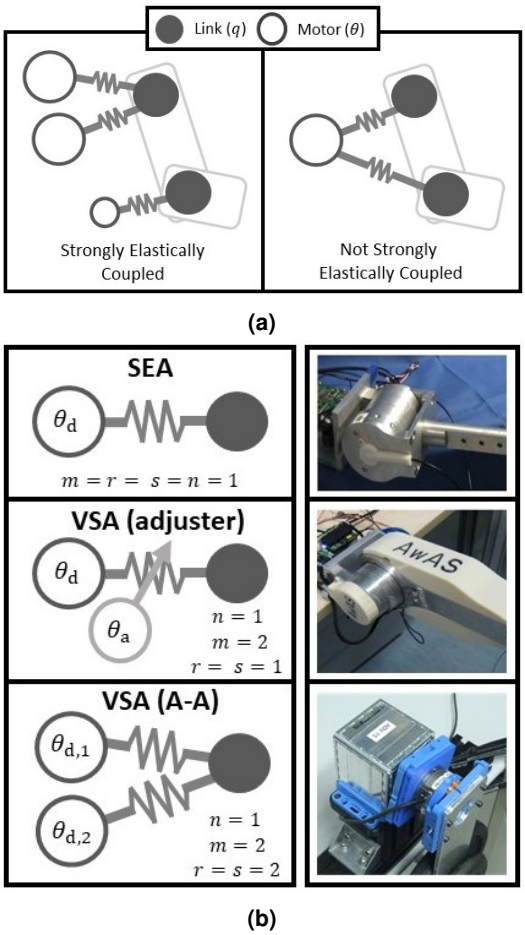

Figure 2. A graphical representation of Definition 1 is reported in (a), while in (b) different schemes of compliant actuators (left-hand side) and pictures of real prototypes (right-hand side) are shown: the CompACT (Tsagarakis et al. 2009) (top), the AwAS (Jafari et al. 2013) (middle) and the VSA-Cube (Catalano et al. 2011) (bottom). Variables in (b) represent: m number of motors (θ), n number of joints (q), r number of deflecting motors (θ_d) and number of elastic elements s. Note that, the number of adjusting motors (θ_a) can be obtained as $m - r$.

requirements stated in Section 2 and avoids drawbacks (i), (ii) and (iii) listed in Section 3.

It is useful to recall that soft robots lie in the class of underactuated systems. The literature proposes different definitions of underactuated systems, e.g., systems with the number of control inputs smaller than the number of DOFs (Spong 1998), or systems that are not able to command an instantaneous acceleration in an arbitrary direction in the joint space (Tedrake 2009). In both definitions, the Lagrangian coordinates can be divided into two types, the collocated variables, that have the dimension of the input vector, and the non-collocated variables. Referring to Spong (1998), the first are the variables whose accelerations can be arbitrarily commanded, while the accelerations of the second can not. In our case, i.e., articulated soft robots, the first variables refer to the motor positions θ, and the second are the link positions q. Indeed, for these systems, the actuation of the joints relies on the elastic elements that connect the links to the motors. Thus, to control the non-collocated variables it is possible to exploit their coupling with the collocated ones. The coupling can derive from the inertial components of the system dynamics, as for the case of strong inertially coupled systems defined in Spong (1998), or may depend on the presence of a potential term that relates the collocated and non-collocated variables, as shown by the potentially coupled condition in Albu-Schäffer and Petit (2012). Furthermore, the potential term can be relative to the gravity effect or associated to the presence of elastic terms. For the latter case, we here introduce a new rigorous definition: *strong elastic coupling*.

4.1 Model decoupling

According to Albu-Schäffer and Petit (2012), we assume that the system is such that there exists a relation between the collocated and the non-collocated state variables in static configurations. This means that it is always possible, for any given external torques $\hat{\tau}_{\text{ext}}$ and link positions $\hat{q}$, to find motor positions $\overline{\theta}$ and corresponding motor torques $\overline{\tau}_{\text{m}}$ that balance external load, i.e., solve (1) and (2) at the equilibrium. More accurately we define the following

Definition 1. *The system (1) and (2) is said to be Strongly Elastically Coupled (SEC) if, $\forall \hat{q}$ and $\hat{\tau}_{\text{ext}}$, $\exists \overline{\theta}$ and $\overline{\tau}_{\text{m}}$ such that, at the equilibrium (i.e., $\ddot{q} = \dot{q} = 0, \ddot{\theta} = \dot{\theta} = 0$), it holds*

$$\left\{ \begin{array}{l} \left.\dfrac{\partial V(q,\theta)^T}{\partial q}\right|_{\hat{q},\overline{\theta}} = \hat{\tau}_{\text{ext}} - G(\hat{q}), \qquad (12) \\ \left.\dfrac{\partial V(q,\theta)^T}{\partial \theta}\right|_{\hat{q},\overline{\theta}} = \overline{\tau}_{\text{m}}. \qquad (13) \end{array} \right.$$

Remark 1. *Definition 1 implies that $\frac{\partial V(\hat{q},\theta)^T}{\partial \hat{q}} : \mathbb{R}^m \to \mathbb{R}^n$, with $m \geq n$, is surjective.*

Definition 1 is graphically explained in Fig. 2a. Hereinafter, we will consider n-DOFs systems with lumped elasticity at the joints, described as in (1) and (2). In the implementation of VSA, it is expedient to distinguish motors which are directly connected to the extreme of one or more elastic elements, each connected in turn to one or more of the links; and motors which are instead explicitly designed to vary the stiffness of the elastic elements. We will term the first type as *deflecting* motors, while the second will be referred to as *adjusting* motors. In general, we assume to have m motors, r of which are deflecting and $m - r$ are adjusting motors. Fig. 2b illustrates this distinction for three different compliant actuators. More precisely we define

Definition 2. *Two or more rigid bodies (motors and/or links) with Lagrangian coordinate $\mu_i, i = 1, \ldots, \ell \geq 2$, are said to be **elastically connected** (or connected for brief) if there exists an elastic element whose potential $V(\cdot)$ depends on their coordinates, i.e., $V(\mu_1, \mu_2 \ldots, \mu_\ell)$, $\frac{\partial V(\cdot)}{\partial \mu_i} \not\equiv 0$, $i = 1, \ldots, \ell$.*

Definition 3. *A motor is said to be a **deflecting** motor and is associated with the Lagrangian variable θ_{d}, if it is elastically connected to $n \geq 1$ links, associated to the Lagrangian variable q_i, $i = 1, ..., n$, and the elastic potentials $V_l(\cdot)$ depend only on the linear combination of θ_{d} and q_i, i.e., $V_i(q_i, \theta_{\text{d}}) = f(\alpha_1 q_i + \alpha_2 \theta_{\text{d}})$ with non-null α_1 and α_2.*

Definition 4. *A motor is said to be an **adjusting** motor and is associated with the Lagrangian variable θ_{a}, if it is elastically connected to $n \geq 1$ links, associated to*

the Lagrangian variable q_i, $i = 1, ..., n$, and the elastic potentials $V_i(\cdot)$ depend on the product of the functions $f(\cdot)$ and $g(\cdot)$ of q_i and θ_a, respectively, i.e., $V_i(q_i, \theta_a) = f(\alpha_1 q_i) g(\alpha_2 \theta_a)$ with non-null α_1 and α_2.

Furthermore, inspired by Hogan (1985) that classifies the muscles of vertebrates in mono-articular and poly-articular depending on the number of joints on which they exert torques, here we define what follows.

Definition 5. *A deflecting motor is called **mono-articular** if it is elastically connected to only one link. Differently, it is said to be **poly-articular.***

Remark 2. *Given Definition 5, we define as mono-articular system a system whose deflecting motors are all mono-articular. We define poly-articular systems all the other cases.*

To realize the motor-link connections, we assume that the system has s total elastic elements. Moreover, it may happen that there exist additional elastic elements connecting multiple deflecting motors (motor-coupling) or, similarly, other elastic interconnections between links (link-coupling). A further definition is useful to state our propositions.

Definition 6. *A system in the form (1) and (2), is said to be **homogeneous** if all the deflecting motors elastically connected to the same links share equal inertia and damping terms.*

It is worth noting that the presence of the $m - r$ adjusting motors does not alter the homogeneity property of the system.

From these definitions, multiple topologies of compliant systems can be realized. Fig. 3 shows, as an example, the case of a system with three deflecting motors (r), two links (n) and different connections of the elastic elements (s). From now on, we will consider the general case in which $s \geq r \geq n$. Note that the SEA is a particular case where $s = r = n$. We let $\theta \in \mathbb{R}^m$ denote the vector of motor positions, and we assume that the motors are ordered so that $\theta = \begin{bmatrix} \theta_d^T & \theta_a^T \end{bmatrix}^T$, where $\theta_d \in \mathbb{R}^r$ and $\theta_a \in \mathbb{R}^{m-r}$ are the motor variables already defined in Definitions 3 and 4, respectively. For convenience, we collect mono-articular (θ_m) and poly-articular (θ_p) components such that $\theta_d = [\theta_m^T \ \theta_p^T]^T$. Then, the following assumption holds in many compliant actuators in practical use. In Appendix C some useful examples are reported.

Assumption 1. *The elastic potential of the system (1) and (2) has the form*

$$V(q, \theta) = \sum_{i=1}^{s} V_i(q, \theta) = \sum_{i=1}^{s} f_i(\overbrace{a_i q + b_i \theta_d}^{y_i}) g_i(\overbrace{c_i \theta_a}^{w_i}), \quad (14)$$

where, for each i: $f_i(\cdot)$ and $g_i(\cdot)$ are functions at least of class $\mathbb{C}^1$; $a_i \in \{-1, 0, 1\}^{1 \times n}$ has non-zero elements corresponding to links connected to the i-th elastic element; $b_i \in \{-1, 0, 1\}^{1 \times r}$ has non-zero elements corresponding to deflecting motors connected to the i-th elastic element, and $c_i \in \{0, 1\}^{1 \times (m-r)}$ has ones corresponding to motors adjusting the i-th elastic element.

From (14) it is possible to observe that the functions $f_i(\cdot)$ rely only on the deflecting components of the motor positions, while the potential term $g_i(\cdot)$ depends only on the adjusting motor position components.

Remark 3. *Under Assumption 1, (12) and (13) can be rewritten as*

$$\begin{cases} \dfrac{\partial V(q,\theta)^T}{\partial q}\Big|_{\hat{q},\bar{\theta}} = A z(q,\theta)|_{\hat{q},\bar{\theta}} = \hat{\tau}_{ext} - G(\hat{q}), & (15) \\ \dfrac{\partial V(q,\theta)^T}{\partial \theta}\Big|_{\hat{q},\bar{\theta}} = \begin{bmatrix} B z(q,\theta) \\ C v(q,\theta) \end{bmatrix}\Big|_{\hat{q},\bar{\theta}} = \begin{bmatrix} \overline{\tau}_d \\ \overline{\tau}_a \end{bmatrix}, & (16) \end{cases}$$

where A, B and C are defined as

$$\begin{aligned} A &\triangleq \begin{bmatrix} a_1^T & \dots & a_s^T \end{bmatrix} \in \{-1, 0, 1\}^{n \times s}, \\ B &\triangleq \begin{bmatrix} b_1^T & \dots & b_s^T \end{bmatrix} \in \{-1, 0, 1\}^{r \times s}, \\ C &\triangleq \begin{bmatrix} c_1^T & \dots & c_s^T \end{bmatrix} \in \{0, 1\}^{(m-r) \times s}, \end{aligned} \quad (17)$$

and the motor torques vector is divided in two components: deflecting torques $\overline{\tau}_d$ and adjusting torques $\overline{\tau}_a$. Observe that the vectors $z(q, \theta)$ and $v(q, \theta)$ represent elastic torque components of the system. From Definition 1 it follows that A and B are full-row-rank. More details about the derivation of the terms $A, B, C, z(q, \theta)$ and $v(q, \theta)$ are reported in Appendix B.

Under this assumption, we can state the following

Proposition 1. *For a SEC system fulfilling Assumption 1 there exist matrices $\Gamma_d \in \mathbb{R}^{n \times r}, \Upsilon \in \mathbb{R}^{n \times p}$ and $\Pi \in \mathbb{R}^{n \times q}$ such that*

$$\hat{\tau}_{ext} - G(\hat{q}) = \Gamma_d \overline{\tau}_d + \Upsilon \lambda_1 + \Pi \lambda_3, \quad (18)$$

where the terms $\lambda_1 \in \mathbb{R}^p, \lambda_3 \in \mathbb{R}^q$ are elastic torque components and Γ_d is a full-row-rank matrix.

Proof. The system of equations in (15) and (16) can be rewritten as

$$\begin{cases} \overbrace{\begin{bmatrix} I_n & \mathbf{0} & -A \\ \mathbf{0} & I_r & -B \end{bmatrix}}^{Y} \begin{bmatrix} \tau_g \\ \overline{\tau}_d \\ z \end{bmatrix} = \mathbf{0}, & (19) \\ \begin{bmatrix} I_{(m-r)} & -C \end{bmatrix} \begin{bmatrix} \overline{\tau}_a \\ v \end{bmatrix} = \mathbf{0}, & (20) \end{cases}$$

where $Y \in \{-1, 0, 1\}^{(n+r) \times (n+r+s)}$, $\tau_g \triangleq \hat{\tau}_{ext} - G(\hat{q})$, and $I_l \in \mathbb{R}^{l \times l}$ are identity matrices of size $l = n, r$ and $(m - r)$, respectively. For conciseness, we omitted the dependency from the parameters in $z(q, \theta)$ and $v(q, \theta)$. Note that, systems (19) and (20) are decoupled. The vector $z \in \mathbb{R}^s$ represents all the solutions of (19) and it can be conveniently expressed as

$$z = Q_1 \lambda_1 + Q_2 \lambda_2 + Q_3 \lambda_3 + Q_4 \lambda_4, \quad (21)$$

where Q_i is a basis of the subspace $\mathcal{S}_i$, and the four subspaces are

- $\mathcal{S}_1 = \{z \mid z \in (\mathrm{Im}(A^T) \cap \ker(B))\}$;
- $\mathcal{S}_2 = \{z \mid z \in (\mathrm{Im}(A^T) \cap \mathrm{Im}(B^T))\}$;
- $\mathcal{S}_3 = \{z \mid z \in (\ker(A) \cap \mathrm{Im}(B^T))\}$;
- $\mathcal{S}_4 = \{z \mid z \in (\ker(A) \cap \ker(B))\}$;

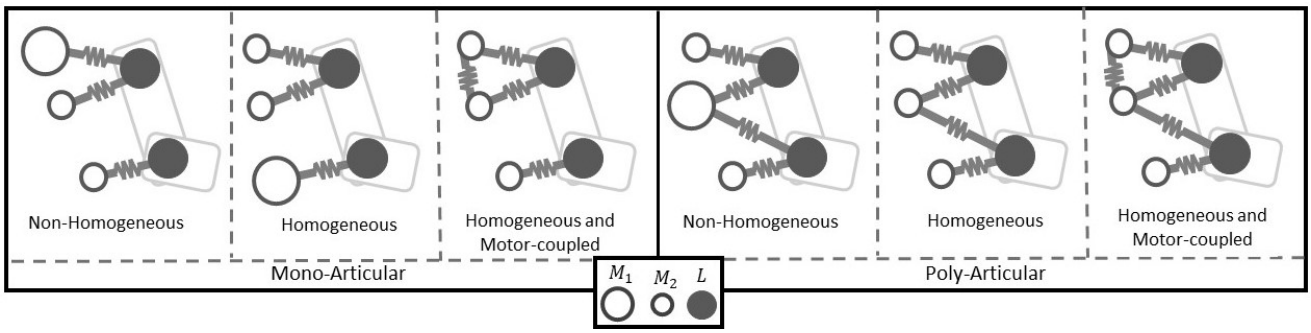

Figure 3. Graphical representation of Definitions 5 and 6 for a SEC system in which there are two links $n = 2$ and three motors $m = 3$, all deflecting $r = m$. Note that the number of elastic connections s varies from 3 (left-hand side in figure) to 5 (right-hand side in figure). The symbol L represents the links and M_i are the motors with inertia and damping J_i, D_i such that $J_1 > J_2$ and $D_1 > D_2$.

such that

$$\begin{aligned}\ker(Y) &= \mathrm{Im}[Q_1 + Q_2 + Q_3 + Q_4] \\ &= \mathcal{S}_1 \oplus \mathcal{S}_1 \oplus \mathcal{S}_3 \oplus \mathcal{S}_4.\end{aligned} \tag{22}$$

Associated to the four subspaces $\mathcal{S}_i$ we have four elastic torque components λ_i. The physical meaning of these torque components is the following: λ_1 are elastic torques that generate link torques without affecting the motor components, λ_2 are elastic torques that generate both link and motor torques, λ_3 are elastic torques that generate motor torques with no effects on the link torques, e.g., co-contraction for A-A systems and λ_4 are elastic components that do not affect either link nor motor torques, i.e., elastic pre-load actions.

Premultipling (21) by the matrix A it is possible to obtain the resulting torques at link side

$$\tau_{\mathrm{g}} = Az = A(Q_1\lambda_1 + Q_2\lambda_2), \tag{23}$$

and, similarly for the motor side, premultipling (21) by the matrix B we obtain

$$\overline{\tau}_{\mathrm{d}} = Bz = B(Q_2\lambda_2 + Q_3\lambda_3). \tag{24}$$

Computing λ_2 from (24) and substituting it in (23) we obtain the thesis

$$\begin{aligned}\tau_{\mathrm{g}} &= AQ_2\left(Q_2^T B^T B Q_2\right)^{-1} Q_2^T B^T \overline{\tau}_{\mathrm{d}} + AQ_1\lambda_1 + \\ &\quad - AQ_2\left(Q_2^T B^T B Q_2\right)^{-1} Q_2^T B^T B Q_3 \lambda_3 \\ &= \Gamma_{\mathrm{d}}\overline{\tau}_{\mathrm{d}} + \Upsilon\lambda_1 + \Pi\lambda_3.\end{aligned} \tag{25}$$

Remark 4. *If the matrices $\Upsilon = \mathbf{0}$, $\Pi = \mathbf{0}$, then (18) simplifies in*

$$\tau_{\mathrm{g}} = \frac{\partial V(\hat{q}, \overline{\theta})^T}{\partial q} = \Gamma_{\mathrm{d}} \frac{\partial V(\hat{q}, \overline{\theta})^T}{\partial \theta} = \Gamma_{\mathrm{d}}\overline{\tau}_{\mathrm{d}}. \tag{26}$$

This is the case, for example, of systems in which $s = r$. Indeed, in this case, the matrix $B = -I \in \mathbb{R}^{r\times r}$ thus, its null-space is the vector $\mathbf{0}$ only, the basis $Q_2 = A^T$ and $\Pi = -AQ_3 \equiv \mathbf{0}$ since $Q_3 \in \ker(A)$. Mono-articular systems are such that (26) is verified. Note that there may be other cases in which the matrices $\Upsilon = \mathbf{0}, \Pi = \mathbf{0}$ even if the matrix $B \neq -I$ and(or) $s \neq r$, e.g., if there are motor-couplings (Tonietti et al. 2005).

Proposition 2. *(Motion/Stiffness decoupling) Consider an ASR with dynamics formulated as in (1) and (2) and elastic potential as in (14). If the system is SEC, homogeneous and Remark 4 holds (i.e., $\Upsilon = \mathbf{0}, \Pi = \mathbf{0}$), then the dynamic model ((1),(2)) can be written in the form*

$$\begin{cases} M\ddot{q} + C\dot{q} + G + \dfrac{\partial V(q, \theta_{\mathrm{eq}}, \theta_{\mathrm{sr}})^T}{\partial q} = \tau_{\mathrm{ext}}, & (27) \\ J_{\mathrm{e}}\ddot{\theta}_{\mathrm{eq}} + D_{\mathrm{e}}\dot{\theta}_{\mathrm{eq}} - \dfrac{\partial V(q, \theta_{\mathrm{eq}}, \theta_{\mathrm{sr}})^T}{\partial q} = \tau_{\mathrm{eq}}, & (28) \\ J_{\mathrm{s}}\ddot{\theta}_{\mathrm{sr}} + D_{\mathrm{s}}\dot{\theta}_{\mathrm{sr}} - \Gamma_{\mathcal{N}}^T \dfrac{\partial V(q, \theta_{\mathrm{eq}}, \theta_{\mathrm{sr}})^T}{\partial \theta} = \tau_{\mathrm{sr}}, & (29) \end{cases}$$

and

$$\begin{bmatrix} \theta_{\mathrm{eq}} \\ \theta_{\mathrm{sr}} \end{bmatrix} \triangleq -\begin{bmatrix} \Gamma\theta \\ \Gamma_{\mathcal{N}}^T\theta \end{bmatrix}, \quad \begin{bmatrix} \tau_{\mathrm{eq}} \\ \tau_{\mathrm{sr}} \end{bmatrix} \triangleq -\begin{bmatrix} \Gamma\tau_{\mathrm{m}} \\ \Gamma_{\mathcal{N}}^T\tau_{\mathrm{m}} \end{bmatrix}, \tag{30}$$

where $\Gamma = [\Gamma_{\mathrm{d}} \ \mathbf{0}] \in \mathbb{R}^{n\times m}$ and $\Gamma_{\mathcal{N}}$ is a basis of the null space of Γ. The terms $J_{\mathrm{e}} \in \mathbb{R}^{n\times n}$, $J_{\mathrm{s}} \in \mathbb{R}^{(m-n)\times(m-n)}$ and $D_{\mathrm{e}} \in \mathbb{R}^{n\times n}$, $D_{\mathrm{s}} \in \mathbb{R}^{(m-n)\times(m-n)}$ are the new inertia and damping matrices of the two equivalent dynamics: the equilibrium dynamics (28) (subscript $_{\mathrm{eq}}$) and the stiffness regulation dynamics (29) (subscript $_{\mathrm{sr}}$). Note that $\tau_{\mathrm{eq}}, \theta_{\mathrm{eq}} \in \mathbb{R}^n$ have the same size of q, while $\tau_{\mathrm{sr}}, \theta_{\mathrm{sr}} \in \mathbb{R}^{m-n}$ have the size of the remaining $m - n$ degrees of actuation.

Proof. Starting from the matrix Γ_{d} computed in Proposition 1 and under Remark 4, we define the full-rank matrix T as

$$T \triangleq \begin{bmatrix} \Gamma \\ \Gamma_{\mathcal{N}}^T \end{bmatrix} \in \mathbb{R}^{m\times m}, \tag{31}$$

where $\Gamma = [\Gamma_{\mathrm{d}} \ \mathbf{0}] \in \mathbb{R}^{n\times m}$ and $\Gamma_{\mathcal{N}}$ is a basis of the null space of Γ. Pre-multiplying the motor dynamics (2) by the matrix T defined in (31) and post-multiplying the matrices J and D by the term $T^{-1}T$ (the identity) we obtain

$$TJT^{-1}T\ddot{\theta} + TDT^{-1}T\dot{\theta} + T\frac{\partial V(q, \theta)^T}{\partial \theta} = T\tau_{\mathrm{m}}. \tag{32}$$

Note that, since the matrix T is full-rank, then its inverse can be written as $T^{-1} = T^T(TT^T)^{-1}$, from which the similarity transformations[‡] TJT^{-1} becomes

$$TJT^{-1} = TJT^T(TT^T)^{-1}. \tag{33}$$

[‡]Hereinafter, we will consider only the transformation in (33). Exact same derivation holds to prove the block diagonal form of the transformation TDT^{-1} thus, we will omit them for the sake of space.

The term TT^T is given by

$$TT^T = \left[\begin{array}{c|c} \Gamma\Gamma^T & \mathbf{0} \\ \hline \mathbf{0} & \Gamma_{\mathcal{N}}^T\Gamma_{\mathcal{N}} \end{array}\right], \tag{34}$$

since $\Gamma\Gamma_{\mathcal{N}} \equiv \mathbf{0}$ and $\Gamma_{\mathcal{N}}^T\Gamma^T \equiv \mathbf{0}$ because $\Gamma_{\mathcal{N}} \in \ker(\Gamma)$. Thus, the inverse of (34) is block diagonal. Instead, the term TJT^T is

$$TJT^T = \left[\begin{array}{c|c} \Gamma J\Gamma^T & \Gamma J\Gamma_{\mathcal{N}} \\ \hline \Gamma_{\mathcal{N}}^T J\Gamma^T & \Gamma_{\mathcal{N}}^T J\Gamma_{\mathcal{N}} \end{array}\right]. \tag{35}$$

To show the block diagonality of (35) we consider the mono-articular case with $m = r$ (all deflecting motors) from which $\Gamma = \Gamma_{\mathrm{d}}$. Then, the matrix Γ can be written as

$$\Gamma = \mathrm{diag}\left(\left[\begin{array}{ccc} \Gamma_1 & \dots & \Gamma_n \end{array}\right]\right), \tag{36}$$

where $\Gamma_j \in \mathbb{R}^{1\times r_j}$ is associated to the j-th link and r_j are the number of motors connected to the j-th link. A basis of the null space of (36) is given by

$$\Gamma_{\mathcal{N}} = \mathrm{diag}\left(\left[\begin{array}{ccc} \Gamma_{\mathcal{N}_1} & \dots & \Gamma_{\mathcal{N}_n} \end{array}\right]\right), \tag{37}$$

where each block $\Gamma_{\mathcal{N}_j} \in \mathbb{R}^{(r_j\times(r_j-1))}$ is chosen as a basis of the null space of each component Γ_j.

Focusing on the off-diagonal elements of (35) it is possible to note that, from (36) and (37) we have

$$\Gamma J\Gamma_{\mathcal{N}} = \mathrm{diag}\left(\left[\begin{array}{ccc} \Gamma_1 J_1\Gamma_{\mathcal{N}_1} & \dots & \Gamma_n J_n\Gamma_{\mathcal{N}_n} \end{array}\right]\right), \tag{38}$$

where $J_j \in \mathbb{R}^{r_j\times r_j}$ is the inertia matrix of the motors associated to the j-th link.

Then, invoking the assumption of homogeneous system each block of (38) can be written as

$$\Gamma_j J_j \Gamma_{\mathcal{N}_j} = J_j\Gamma_j\Gamma_{\mathcal{N}_j} = 0, \tag{39}$$

since $\Gamma_{\mathcal{N}_j} \in \ker(\Gamma_j)$. Matrix (35) is thus block diagonal. These considerations can be extended to the case of compliant systems with $r < m$ by showing that the $m - r$ adjusting components do not affect the computation of Γ. As a consequence, their inertia (and damping) terms can be different w.r.t. inertia and damping of the deflecting motor components.

Finally, from (33), (34), (35) and under (39) we define the matrix

$$\mathcal{J} \triangleq TJT^{-1} = \left[\begin{array}{c|c} J_{\mathrm{e}} & \mathbf{0} \\ \hline \mathbf{0} & J_{\mathrm{s}} \end{array}\right], \tag{40}$$

where $J_{\mathrm{e}} \triangleq \Gamma J\Gamma^T(\Gamma\Gamma^T)^{-1}$ and $J_{\mathrm{s}} \triangleq \Gamma_{\mathcal{N}}^T J\Gamma_{\mathcal{N}}(\Gamma_{\mathcal{N}}^T\Gamma_{\mathcal{N}})^{-1}$. (Exact same derivation holds for $\mathcal{D}$). From (40), (32) becomes equivalent to

$$\mathcal{J}T\ddot{\theta} + \mathcal{D}T\dot{\theta} + T\frac{\partial V(q,\theta)^T}{\partial\theta} = T\tau_{\mathrm{m}}. \tag{41}$$

Given the block diagonality of $\mathcal{J}$ and $\mathcal{D}$, then (41) can be rewritten also as

$$\left\{\begin{array}{l} J_{\mathrm{e}}\Gamma\ddot{\theta} + D_{\mathrm{e}}\Gamma\dot{\theta} + \Gamma\dfrac{\partial V(q,\theta)^T}{\partial\theta} = \Gamma\tau_{\mathrm{m}} \\ J_{\mathrm{s}}\Gamma_{\mathcal{N}}^T\ddot{\theta} + D_{\mathrm{s}}\Gamma_{\mathcal{N}}^T\dot{\theta} + \Gamma_{\mathcal{N}}^T\dfrac{\partial V(q,\theta)^T}{\partial\theta} = \Gamma_{\mathcal{N}}^T\tau_{\mathrm{m}} \end{array}\right., \tag{42}$$

and, substituting (30) in (42) and using (26) (recalling that $\Gamma_{\mathrm{d}} = \Gamma$), the thesis is obtained.

Remark 5. *If the motor dynamics in (28) is negligible or is compensated by the motor actions, then (27), (28) and (29) are simplified in*

$$\left\{\begin{array}{ll} M\ddot{q} + C\dot{q} + G - \tau_{\mathrm{eq}} = \tau_{\mathrm{ext}}, & (43) \\ -\dfrac{\partial V(q,\theta_{\mathrm{eq}},\theta_{\mathrm{sr}})^T}{\partial q} = \tau_{\mathrm{eq}}, & (44) \\ J_{\mathrm{s}}\ddot{\theta}_{\mathrm{sr}} + D_{\mathrm{s}}\dot{\theta}_{\mathrm{sr}} - \Gamma_{\mathcal{N}}^T\dfrac{\partial V(q,\theta_{\mathrm{eq}},\theta_{\mathrm{sr}})^T}{\partial\theta} = \tau_{\mathrm{sr}}. & (45) \end{array}\right.$$

Under Remark 5, (43) represents the dynamics of a flexible joints robot with nonlinear springs, whose elastic torques are determined by τ_{eq}. Furthermore, it is useful to give the physical meaning of the torque components shown in the right-hand side of (44) and (45). The first one, i.e., τ_{eq}, represents the torque components that equate the dynamics of the equivalent flexible joint system at the equilibrium, thus that drives θ_{eq}. Recalling that the motor positions vector is partitioned as $\theta = \left[\theta_{\mathrm{d}}^T \;\; \theta_{\mathrm{a}}^T\right]^T$ and the matrix $\Gamma = [\Gamma_{\mathrm{d}} \;\; 0]$, τ_{eq} results in a combination of the deflecting motor torques only, as described in (30). On the other hand, the torque components τ_{sr} control the dynamics of θ_{sr}. Given (30), it results that the component θ_{sr} are orthogonal to θ_{eq}, and analogously the component τ_{sr} are orthogonal to τ_{eq}. This implies that τ_{sr} does not influence the equilibrium positions θ_{eq}. In addition, given the aforementioned partitioning of the motor positions vector, and consequently of the matrix Γ, the term τ_{sr} also includes torque components that are relative to the adjusting motors. Finally, it is worth noting that (45) may be used to shape the desired feature of the elastic characteristic $V(q,\theta_{\mathrm{eq}},\theta_{\mathrm{sr}})$. Thus, given τ_{eq}, if θ_{sr} is adjusted then θ_{eq} changes in such a way that (44) remains valid.

4.2 Torque-based ILC (tILC) strategy

Assuming that both Proposition 2 and Remark 5 can be applied, then the ASR dynamics (1) and (2) can be rewritten in the form (43), (44) and (45). As previously mentioned, under these assumptions, the two torque actions τ_{eq} and τ_{sr} allow to separately control q and θ_{sr}, respectively. Also, it is worth mentioning that, the considerations made in Section 4.1 hold for a wide variety of actuators, and it is straightforward to compute the matrix Γ_j for two major classes: $\Gamma_j = [-1, \; -1]$ for the case of symmetric A-A VSAs and $\Gamma_j = [-1, \; 0]$ for the case of VSAs with adjuster. More details can be found in Appendix C.

Several control methods could be employed to compute the two torque terms. Here we propose a novel control scheme able to overcome points (i), (ii), (iii). This consists in:

- exploiting τ_{sr} to let θ_{sr} follow a desired trajectory $\hat{\theta}_{\mathrm{sr}}$;
- learning a control action τ_{eq} (consisting of a dominant feedforward component) via an ILC approach to let q follow a desired link-position trajectory $\hat{q}$.

4.2.1 Stiffness adjusting : From (45) the dynamics of θ_{sr} can be interpreted as a linear second order dynamics with a disturbance term $d(q,\theta_{\mathrm{eq}},\theta_{\mathrm{sr}}) = -\Gamma_{\mathcal{N}}^T\frac{\partial V(q,\theta_{\mathrm{eq}},\theta_{\mathrm{sr}})^T}{\partial\theta}$, such that

$$J_{\mathrm{s}}\ddot{\theta}_{\mathrm{sr}} + D_{\mathrm{s}}\dot{\theta}_{\mathrm{sr}} + d(q,\theta_{\mathrm{eq}},\theta_{\mathrm{sr}}) = \tau_{\mathrm{sr}}\,. \tag{46}$$

Thus, to set a desired vector $\hat{\theta}_{\text{sr}}$, rejecting the disturbance d, we choose the following proportional integral (PI) controller

$$\tau_{\text{sr}} = k_{\text{p}}(\hat{\theta}_{\text{sr}} - \theta_{\text{sr}}) + k_{\text{i}} \int (\hat{\theta}_{\text{sr}} - \theta_{\text{sr}}) \text{d}t \ , \tag{47}$$

where $k_{\text{p}}, k_{\text{i}} \in \mathbb{R}$ are the proportional and integral gains.

4.2.2 Motion control : In this part, we design the control action τ_{eq} that enables the robot to track, in t_{f} seconds, a desired link trajectory $\hat{q} : [0, t_{\text{f}}) \to \mathbb{R}^n$, while preserving its compliant behavior (point (ii)) and employing a model-free method (point (i)). Since high-gain feedback control techniques have the drawback of stiffening the robot, in Della Santina et al. (2017a) it is suggested to prefer feedforward control approaches. Among all the possible techniques, we decide to exploit the benefits of the Iterative Learning Control (ILC). Given a desired link trajectory and without the knowledge of the system dynamics, this control strategy is able to achieve good tracking performance by iteratively refining the control action. The iteratively learned control action τ_{eq}, at iteration $k \in \mathbb{N}^+$, combines a FeedForward (FF) and a FeedBack (FB) component, namely τ^k_{FF} and τ^k_{FB}, such that

$$\tau^k_{\text{eq}}(t) = \underbrace{\tau^{k-1}_{\text{eq}}(t) + K_{\text{UP}}(t)\xi^{k-1}(t)}_{\tau^k_{\text{FF}}(t)} + \underbrace{K_{\text{FB}}(t)\xi^k(t)}_{\tau^k_{\text{FB}}(t)} , \tag{48}$$

where the tracking error at iteration k is defined as

$$\xi^k(t) \triangleq \begin{bmatrix} \hat{q}_1(t) - q^k_1(t) \\ \dot{\hat{q}}_1(t) - \dot{q}^k_1(t) \\ \cdots \\ \hat{q}_n(t) - q^k_n(t) \\ \dot{\hat{q}}_n(t) - \dot{q}^k_n(t) \end{bmatrix} \in \mathbb{R}^{2n}, \tag{49}$$

and $K_{\text{UP}}, K_{\text{FB}}$ are the iteration-constant and time-dependent update and feedback control gain matrices, respectively. For the sake of clarity, hereinafter, the time dependency will be omitted whenever possible. Note that, in order to preserve the robot's compliant behavior, τ^k_{FB} should remain small, while most of the total control action should rely on τ^k_{FF}.

To be independent of the dynamics of the system, overcoming problem (i) and simplifying the selection of the control gains in (48), we employ a decentralized[§] control approach (Siciliano et al. 2010). Thus, the control matrices can be written as $K_{\text{UP}} \triangleq \text{diag}(K_{\text{UP},j}) \in \mathbb{R}^{n \times 2n}$ and $K_{\text{FB}} \triangleq \text{diag}(K_{\text{FB},j}) \in \mathbb{R}^{n \times 2n}$, where $K_{\text{UP},j} \triangleq [K_{\text{pUP},j} \ \ K_{\text{vUP},j}] \in \mathbb{R}^{1\times 2}$ are the update gains relative to the position (subscript $_{\text{p}}$) and velocity (subscript $_{\text{v}}$) error, and $K_{\text{FB},j} \triangleq [K_{\text{pFB},j} \ \ K_{\text{vFB},j}] \in \mathbb{R}^{1\times 2}$ are the feedback gains (again relative to position and velocity error) of the j-th joint. It is worth noting that, without loss of generality, we can rewrite (43) as

$$\dot{z}_j = \underbrace{\begin{bmatrix} 0 & 1 \\ 0 & -L_j/W_j \end{bmatrix}}_{E_j} z_j + \underbrace{\begin{bmatrix} 0 \\ 1/W_j \end{bmatrix}}_{H_j} \tau_{\text{eq},j} + \delta_j(z, \dot{z}), \tag{50}$$

where $z_j = [q_j, \ \dot{q}_j]^T$ is the state, W_j and L_j are the inertial and damping coefficients for the j-th joint, respectively. $\delta_j(z, \dot{z})$ collects friction, uncertainties, gravitational components and coupling terms between joints. Note that W_j and L_j can be firstly identified with a step response, resulting in scalar constants, while $\delta_j(z, \dot{z})$ is state-dependent. The state matrix E_j and the input vector H_j are also constants.

To guarantee the convergence of the iterative learning process, we leverage on the criteria introduced in Ouyang et al. (2011) and adopted in Angelini et al. (2018), that refer to a dynamic system in the from $\dot{x} = f(x) + Bu + \nu$, where x, u and ν are the state, control input and uncertainties vectors, respectively and f, B are the drift vector and the input matrix. Adopting a control technique as in (48), the convergence of the method is guaranteed if the following conditions are satisfied

$$\left\| (I + K_{\text{FB}}(t)B)^{-1} \right\|_\infty < 1, \forall t \in [0, t_{\text{f}}), \tag{51}$$

$$\left\| I - K_{\text{UP}}(t)B \right\|_\infty < 1, \forall t \in [0, t_{\text{f}}), \tag{52}$$

where $\|\cdot\|_\infty$ stands for the ∞-norm (Ouyang et al. 2011).

The convergence conditions (51) and (52), applied to (50), become

$$\left| (1 + K_{\text{FB},j}(t)H_j)^{-1} \right| < 1, \forall t \in [0, t_{\text{f}}), \tag{53}$$

$$|1 - K_{\text{UP},j}(t)H_j| < 1. \tag{54}$$

The feedback gain $K_{\text{FB},j}(t)$ is chosen as the solution of the following time-varying linear quadratic optimization problem $\int_0^{t_{\text{f}}} z_j^T Q z_j + R\tau^2_{\text{eq},j} \text{d}t$, with $R \in \mathbb{R}^+$ and $Q \in \mathbb{R}^{2\times 2}$ design parameters. Thus,

$$K_{\text{FB},j}(t) = R^{-1} H_j^T S_j(t), \tag{55}$$

with $S_j(t) \in \mathbb{R}^{2\times 2}$ solution of the time-varying matrix Riccati differential equation, i.e., $\dot{S}_j = -S_j E_j - E_j^T S_j + S_j H_j R^{-1} H_j^T S_j - Q$ (constrained by $S_j(t_{\text{f}}) = \mathbf{0}$).

For the update component we adopt the following choice

$$K_{\text{UP},j}(t) = (1 + \epsilon) H_j^\dagger + \Phi_j, \tag{56}$$

where $H_j^\dagger$ is the Moore-Penrose pseudoinverse of the matrix H_j, ϵ is chosen as $\epsilon = 0.9$ (Angelini et al. 2018) and $\Phi \in \mathbb{R}^{1\times 2}$ is a vector to be chosen such that $\Phi_j^T \in \ker(H_j^T)$.

Then, we state the following

Proposition 3. *For the system in (50) controlled by (48), if, for each joint j the feedback control gain $K_{\text{FB},j}$ is chosen as (55) and the update gain $K_{\text{UP},j}$ as (56), then, $\forall \epsilon \in [0, 1), \forall \Phi_j^T \in \ker(H_j^T)$ and $\forall R > 0$, the convergence of the iterative algorithm is guaranteed.*

Proof. By choosing $K_{\text{FB},j}$ as in (55), condition (53) becomes

$$\left| \frac{R}{R + H_j^T S_j(t) H_j} \right| < 1, \ \forall t \in [0, t_{\text{f}}), \tag{57}$$

that is always fulfilled $\forall R > 0$ because $H_j^T S_j(t) H_j$ is always positive definite. This is true since H_j is a non-null vector (inertia term) and $S_j(t)$ is positive definite by definition.

[§] According to this approach we can rewrite the inertia and damping matrix in (43) as $M = W + \Delta W$ and $C = L + \Delta L$, with $W = \text{diag}(W_j)$, $L = \text{diag}(L_j)$ and rewrite the dynamics of the j-th joint as in (50), collecting the coupling terms in $\delta(z, \dot{z})$.

Algorithm 1 Control scheme pseudo-code

procedure INITIALIZATION
  $Set(\hat{q}(t), \dot{\hat{q}}(t), \ddot{\hat{q}}(t))$ ▷ Desired joint trajectory
  $Set(\hat{\theta}_{\text{sr}}(t))$ ▷ Stiffness profile selection
  $Set(k_{\text{p}}, k_{\text{i}})$ ▷ s.r.p. PI loop gains
  $Set(Q, R)$ ▷ LQR control parameters
  $Compute(\tau^0_{\text{FF}})$ ▷ Initial guess Eq. (60)
  $Evaluate(K_{\text{FB}}(t), K_{\text{UP}}(t))$ ▷ ILC gains Eq. (55), (56)
procedure LEARNING
  $k \leftarrow 1$ ▷ Iteration number
  $\xi^{k-1}(t) \leftarrow 0$ ▷ Tracking error (49)
  do
    $Run\_Trial(\tau^{k-1}_{\text{eq}})$
    $Store(e^k, \xi^k, \tau^k_{\text{eq}})$
    $Update(\tau^k_{\text{eq}})$
    $k \leftarrow k + 1$
  while $e^{k-1} > threshold$ ▷ Iteration error (63)

For the second condition (54), indeed, by substituting (56) in (54) we obtain

$$\begin{aligned} |1 - K_{\text{UP},j} H_j| &< \left|1 - (1+\epsilon) H_j^{\dagger} H_j + \Phi_j H_j\right| \\ &< |\epsilon - \Phi_j H_j| < |\epsilon| < 1, \end{aligned} \tag{58}$$

that is always verified with the assumptions made of $\epsilon \in [0, 1)$ and $\Phi_j^T \in \ker(H_j^T)$.

Remark 6. *Since $H_j = [0 \;\; W_j^{-1}]^T$, we obtain that $\Phi_j = [K_{\text{pUP},j} \;\; 0]$. Then, according to Angelini et al. (2018), in order to maintain the same balance between proportional gain on position and proportional gain on velocity of the j-th joint, we impose the following*

$$K_{\text{pUP},j} = \frac{\|K_{\text{pFB},j}(t)\|_1}{\|K_{\text{vFB},j}(t)\|_1} K_{\text{vUP},j}, \forall j = 1, \dots n, \tag{59}$$

where $\|\cdot\|_1$ is the 1-norm of the vector.

In order to apply the proposed iterative strategy, an initial guess for the FF torque reference is needed. To compute it, the steps followed are the same as implemented in the pILC strategy in Angelini et al. (2018). Thus, for the j-th joint, given the coefficients W_j and L_j previously defined and a desired trajectory, with its first and second derivatives $(\hat{q}_j,\ \dot{\hat{q}}_j,\ \ddot{\hat{q}}_j)$, the initial guess is computed as

$$W_j \ddot{\hat{q}}_j + L_j \dot{\hat{q}}_j + \tau_{\text{g},j}(0) = \tau^0_{\text{FF},j}, \tag{60}$$

where the term $\tau_{\text{g},j}(0)$ is the torque needed to hold the j-th joint at initial position, i.e., at the time instant $t = 0$.

In conclusion, learning the control action τ_{eq} with the tILC approach allows to track the desired position profile with no knowledge of the system model (point (i)), while, as a result of Proposition 2, the term τ_{sr} is used to separately (point (iii)) adjust the stiffness of the system, overcoming point (ii). The overall control scheme is shown in Fig. 4, while in Algorithm 1 the pseudo-code for the implementation is reported.

Remark 7. *The stability analysis of the closed-loop system (1) and (2) with the control inputs given by (47) and (48) during each iteration requires further discussion. The problem amounts to studying the stability of a flexible joints robot around a time-varying trajectory. To the best of the authors' knowledge, this problem, in its most general form, has not been solved yet. However, the following considerations apply:*

- *in case of perfect knowledge of the system model, the techniques presented in the S.o.A. (Section 3) can be exploited to solve the tracking problem in a stable manner;*
- *in case of partially unknown model, but perfect knowledge of the gravitational term, asymptotic stability can be ensured. Tomei (1991) proves the stability of an equilibrium point. De Luca and Book (2016) show that the system can be locally stabilized around a slowly varying reference trajectory;*
- *in case of a non-perfect knowledge of the gravitational term, asymptotic stability is still guaranteed, but at a different equilibrium point (Tomei 1991);*
- *for the general case of non-perfect knowledge of the system model, flexible joints robots and time-varying trajectories, there are no results in the literature yet. However, it is reasonable to think that, if the reference trajectory varies slowly, marginal stability may be achieved by employing similar assumptions of (Tomei 1991).*

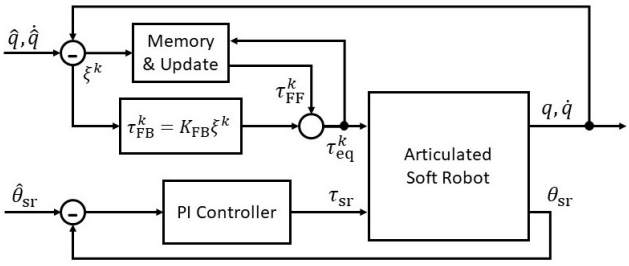

Figure 4. Control scheme of the tILC strategy

By choosing the control gains as shown in Section 4 and by assuming a reference trajectory slowly varying over time, the control method presented in this work lies in the last aforementioned case. Note that, although the stability is not proven, no stability issues have been encountered during the experimental validation presented in Section 5. Future work will address the theoretical proof for this last case.

4.3 From theory to application

In practical implementations, some of the hypotheses that underlay the proposed control scheme could be not fulfilled. In this section, we discuss the role of these hypotheses on the controller performances and possible solutions to overcome the case in which they are not verified.

First of all, this work considers the case of compliant systems with lumped elasticity concentrated at the joint. For each joint, the number of motors should be greater or equal than one, and at least one motor has to be elastically connected to the link. This guarantees that the system satisfies Definition 1. If the elasticity is distributed on the structure, e.g., in the case of continuum soft robots, then

there are two consequences: the dynamic model of the system changes and the definition of the link positions should be revisited. Approximation methods can be considered to overcome these two points, e.g., (Della Santina and Rus 2019) or (Yu et al. 2018). Consequently, to fruitfully apply the elastic coupling concept to a discrete model of continuum soft robots, Definition 1 may necessitate a generalization.

To prove Proposition 2, the system is assumed to be homogeneous. However, it may happen that nominally equal motors are slightly different from one another, e.g., because of production tolerances. Experimental results reported in Section 5 show that the motion/stiffness decoupling can be done even if there are small differences in the dynamics of the motors coming from the manufacturing process. Differently, for other types of non-homogeneous systems, such as A-A systems with different motor dynamics, a more detailed analysis has to be pursued, e.g., considering the knowledge of the motor model. Reliable knowledge of the motor model can also be helpful to compensate motor dynamics when they are not negligible, i.e., when Remark 5 is no more valid.

The elastic potential should be reconducted in the form of Assumption 1 in order to apply Proposition 1. Then, Remark 4 (e.g., the case of mono-articular systems) has to be verified to apply Proposition 2. If this is not the case, then the motion/stiffness decoupling can not be performed since coupling terms appear between link-side and motor-side dynamics. Appendix C shows that Assumption 1 holds true in many compliant actuators presented in the literature. However, there may be cases of systems in which the method can be still applied even if this assumption is relaxed. For instance, in the case of systems with only one poly-articular motor it is possible to prove the decoupling property following the same steps of Section 4 (not reported here for the sake of space). Other cases will be investigated in future works.

Furthermore, in realistic elastic connections, the statement in Remark 1 together with the assumption of constant external disturbances of the ILC approach may not hold because of the presence of Coulomb friction. The presence of these phenomena may alter the convergence to zero of the iterative process. Indeed, Wang and Longman (1994) show that stick-slip friction may lead to a limit cycle like behavior that degrades the learning results. According to Wang and Longman (1994), to take into account this effect it is possible to include a torque friction contribution (τ_{fc}) on the flexible joint robot dynamics[¶] that becomes

$$\begin{cases} M\ddot{q} + C\dot{q} + G - \tau_{\text{eq}} = \tau_{\text{ext}} - \tau_{\text{fc}}, & (61) \\ -\dfrac{\partial V(q, \theta_{\text{eq}}, \theta_{\text{sr}})^T}{\partial q} = \tau_{\text{eq}}, & (62) \end{cases}$$

In this case, there are two possible consequences:

- The convergence of the learning process is no more guaranteed and typically the tracking error may start to oscillate around a mean value. This occurs because at each iteration one specific friction contribution is learned. However, this contribution varies through iterations, i.e., $\tau_{\text{fc}}^{k+1} \neq \tau_{\text{fc}}^{k}$.
- If τ_{fc} depends on θ_{sr}, then the use of a feedforward action that has learned $\bar{\theta}_{sr}$ will be subject to an error if employed to track the same desired trajectory with $\hat{\theta}_{sr} \neq \bar{\theta}_{sr}$.

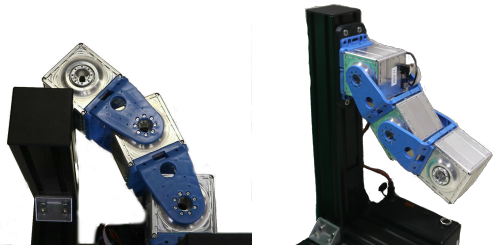

(a) Horizontal configuration during impact (top view).

(b) Vertical configuration: subject to gravity.

Figure 5. The *2*-DOF structures equipped with VSAs and used as experimental setup to evaluate the stiffness preservation (5.3).

The influence of these two facts on the experimental results is discussed in Section 5. To cope with these problems, friction compensation techniques may be implemented, e.g., following Papadopoulos and Chasparis (2004). This solution will be analyzed in future works.

5 Experimental validation

In this section the control strategy proposed in Section 4 is experimentally validated on different compliant robotic structures, each of them is equipped with symmetric A-A VSAs at the joints. For these actuators both Proposition 1 and Remark 4 are verified, thus the motion/stiffness decoupling (Proposition 2) can be applied.

A first experimental example (*Comparative example*) compares the results of the proposed control scheme with S.o.A. control strategies and motivates the choice of an iterative learning approach. The comparison is made by means of the average tracking error at the joints and aims to prove that the proposed method allows to track the desired trajectory.

Furthermore, in another experiment (*Motion/Stiffness decoupling*) the iterative approach is used to learn a torque control action suitable to track the desired trajectory with the desired stiffness profile. Then, the compliant behavior is changed through the s.r.p., and the tracking error is evaluated again. At this point, differently from the first experiment, our intention is to evaluate the deviation of the tracking error that occurs after the change of stiffness (i.e., the gap). Then, with this experiment, we want to prove the motion/stiffness decoupling described in Section 4.1: the main contribution of the control strategy proposed in this paper. The experimental results show that, using this control action and different s.r.p. (i.e., compliant behaviors), the trajectory tracking can be still performed with a small error, proving the decoupling. The validity of this result is demonstrated both on a simple *2*-DOF structure placed in a vertical configuration (Fig. 5b) and on a more complex *6*-DOF robotic arm described in Appendix D and shown in Fig. 1 and Extension 1. These

[¶]Note that friction effects on the adjusting dynamics (45) will be compensated by the control loop.

results are compared to the results obtained with the pILC strategy (Section 3).

Finally, a third experiment (*Stiffness preservation*) is executed to effectively prove the preservation of the imposed stiffness behavior. This is verified through an impact test. It is worth noting that, for the chosen test-bed, the stiffness computation strictly depends on the load applied at the link. Two cases are investigated: with and without external load. Fig. 5a depicts the structure with no external disturbances at the moment of impact, while Fig. 5b shows a case in which the gravity contribution is not negligible.

For all the structures of the experiments, the low-level PI gains (47) of the actuators are set as $k_{\mathrm{p}} = 0.5$ and $k_{\mathrm{i}} = 0.005$. The internal firmware of the actuators runs at 1kHz. More details about the test-bed are reported in Appendix D.

5.1 Comparative experimental analysis

In this example, we analyze and compare the performance of our tILC strategy with other three S.o.A. control methods: 1) a computed torque with PID on the equilibrium position of the motor, i.e. θ_{eq} (CT-PID$_\theta$), proposed in (De Luca 2000); 2) a computed torque with PID on the link position (CT-PID$_{\mathrm{q}}$); 3) a PID law on the link position (PID$_{\mathrm{q}}$). It is worth noting that the first two techniques are model-based, while the simple PID$_{\mathrm{q}}$ and the one proposed here are model-free.

The experimental setup is a 1-DOF planar structure made with one VSA, obtained by removing the second joint from the system shown in Fig. 5a (without obstacle). The reference link trajectory is a five order minimum jerk step from zero to $q(t_{\mathrm{f}}) = 60$deg in $t_{\mathrm{f}} = 6$s, as shown in Fig. 6a (dashed black line). For all the four strategies we imposed a constant stiffness regulation parameter $\theta_{\mathrm{sr}} = 0.5\Delta_{\mathrm{m}}$rad, with Δ_{m} maximum s.r.p. allowable for the joint.

To design the control gains of the PID controllers for the three techniques, an optimization problem has been solved using as cost function the error in (63). The values (P,I,D) obtained are the following: $k_1 = [2.7e03,\ 9.4e\text{-}03,\ 22.6]$ and $k_2 = k_3 = [2.5e03,\ 4.0e\text{-}03,\ 75.4]$.

Results: In Table 1 and Fig. 6 the comparative results are reported. Figure 6a shows the link tracking and the equilibrium position tracking of the four analyzed methods. The error evolution for 20 iterations of the tILC method (solid orange line) and 20 consecutive trials of the other control strategies (solids green, violet, and yellow lines) is illustrated in Fig. 6b.

The first result to observe is that, once the iterative process converges (from iteration 10), the tracking error for the tILC case is lower compared to the other methods (see Fig. 6b). More in details, the simple PID$_{\mathrm{q}}$ gives worst performances compared to the tILC strategy. Nevertheless, due to the simple case under analysis (i.e. planar 1-DOF), for which we can easily evaluate the dynamic model parameters, if

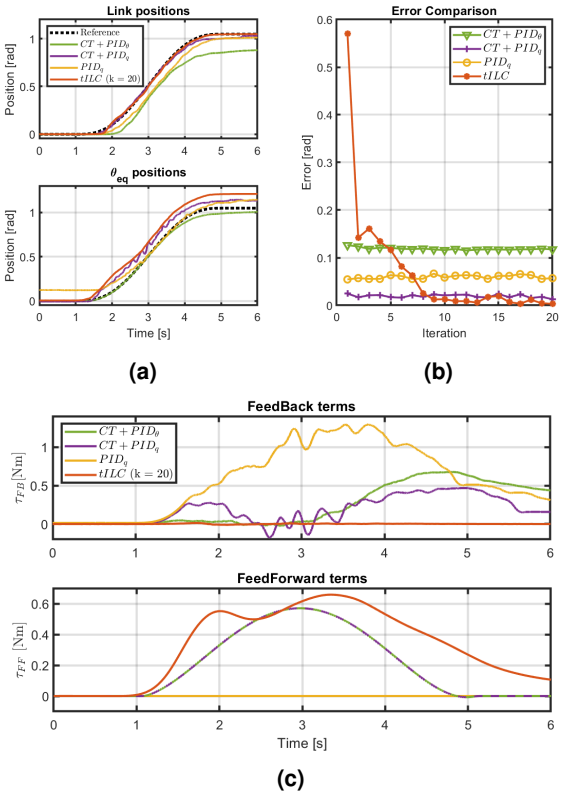

Figure 6. Graphical results of the comparative experiment. Trajectory tracking for both link and equilibrium position are reported in (a), top and bottom plot, respectively. The evolution of the error (eq. (63)) during iterations (for tILC) and during different trials (for the other controls) is reported in (b), while comparison between FB and FF torque components is shown in (c). Note that, for the tILC case in (a) and (c) we considered the last iteration ($k = 20$).

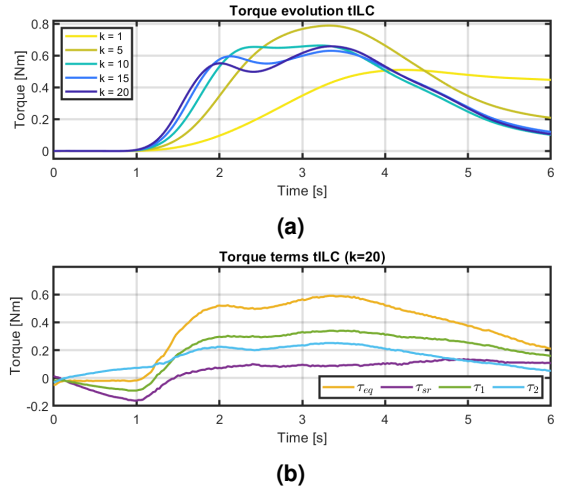

Figure 7. The evolution of the equilibrium torque τ_{eq} through iterations is shown in (a), while the plot in (b) shows the measured motor torques at the last iteration $k = 20$ together with the equilibrium and the stiffness regulation contributions, for the tILC method in the 1-DOF case.

Strategy	$\bar{e}_I$[rad]	Δe_I[rad]	$\int \tau^2_{\mathrm{FB}}$[Nm]	$\int \tau^2_{\mathrm{FF}}$[Nm]
CT+PID$_\theta$	0.117	0.001	0.123	0.088
CT+PID$_{\mathrm{q}}$	0.020	0.004	0.062	0.088
PID$_{\mathrm{q}}$	0.060	0.003	0.538	-
tILC	0.009	0.005	1.6e-05	0.164

Table 1. Numerical results for the four strategies. The first two columns report the mean and the standard deviation of the error for the last ten iterations/trials, i.e. $I \in [10:20]$. The value of the torque power index for the components of FB and FF is shown in the last two columns. Note that the PID$_{\mathrm{q}}$ has, obviously, no FF term.

we add a feedforward model-dependent term (CT+PID$_q$ method) we can obtain good tracking results. It is worth noting, however, that the sole use of the model-dependent term, closing the feedback loop on the equilibrium position of the motors (CT+PID$_\theta$), is not sufficient to achieve good results. This is due to the fact that, despite the simple case, the model does not perfectly match with the real system. Consequently, the control strategies analyzed should leverage the feedback terms to reach good tracking performance. Then, as discussed in Section 1, in this last situation the compliant behavior may be altered. The evolution of FB and FF torque components are shown in Fig. 6c and their amount are reported in Table 1 (last two columns).

This point introduces the second important result of this comparative example. Indeed, it is possible to see how, among all the other strategies, tILC allows us to achieve the best tracking performance (Fig. 6a top plot) maintaining the feedback component to a minimum amount (Fig. 6c bottom plot, orange line). This can also be verified in Table 1.

Furthermore, for the tILC strategy proposed in this work, the evolution of the feedforward contribution τ_{eq} through iterations is reported in Fig. 7a, while all the measured torque contributions are shown in Fig. 7b.

5.2 Motion/Stiffness decoupling

These experiments aim to prove the decoupling of the proposed strategy compared to the results obtained with the pILC approach (Angelini et al. 2018). The two ILC approaches employ the same control parameter R and start from the same rough estimation of the dynamic parameters, obtained through a step response.

The experiments proceed as follow:

- **learning process**; according to the ILC case under test, in this phase an equilibrium torque τ_{eq} (or position θ_{eq}) control action is learned through iterations with a specific compliant behavior (*soft* or *stiff*). The iterations proceed until the trajectory tracking error reaches a satisfying value,
- **stiffness change**; once the control action is learned, the stiffness regulation parameter θ_{sr} is changed to modify the compliant behavior, from low value (*soft*) to high value (*stiff*), and viceversa. The same control action is used to execute one more iteration, and the overall tracking error[‖] is computed as

$$e^k \triangleq \frac{\sum_{j=1}^{n} \left(\int_0^{t_\text{f}} \left| \hat{q}_j - q_j^k \right| \text{d}t \right)}{n \cdot t_\text{f}}, \tag{63}$$

  where k is the iteration number, t_f final time and n number of joints,
- **performance recovery**; additional iterations are performed to recover the trajectory tracking performance degradation caused by the stiffness transition.

5.2.1 2-DOF (vertical configuration) : For this simple case the joint trajectory goes from $q(0) = [0, 0]^T$deg to $q(t_\text{f}) = [35, 45]^T$deg in $t_\text{f} = 2$s. The reference trajectory is a five order minimum jerk trajectory. The stiffness regulation parameters are set as $\theta_{\text{sr},j} = 0.2\Delta_{\text{m},j}$ for the soft case and $\theta_{\text{sr},j} = 0.8\Delta_{\text{m},j}$ for the stiff case, where $\Delta_{\text{m},j}$ is the maximum s.r.p. for the *j*-th actuator. For both ILC approaches the control parameters are chosen as $R = 5$.

Results: Fig. 8 shows the evolution of e^k for both position (dashed blue line) and torque (solid orange line) ILC, either for the soft to stiff transition (Fig. 8a), and the stiff to soft transition (Fig. 8b). Table 2 reports the numerical results. For these cases 20 iterations are required to reach a small tracking error with both the behaviors (left-hand side curves of the plots in Fig. 8a and Fig. 8b). From the $21st$ on iteration the s.r.p. is changed and other 20 iterations are performed (right-hand side curves of the plots in Fig. 8a and Fig. 8b). In both the figures, FF20 refers to the error at the $20th$ iteration (e^{20}) while FF20+1 refers to the first iteration after the stiffness change, starting from FF20 (e^{21}). It is worth noting that, comparing the FF20 and FF20+1 marked points in both the cases of Fig. 8a and Fig. 8b, the gaps relative to the pILC case (blue square markers) are larger then the gaps of the tILC case (orange circle markers). More in detail, the ratio between the error gaps in the tILC case and the error gap in the pILC case is: 0.50, for the soft to stiff case (Fig. 8a) and 0.45, for the stiff to soft (Fig. 8b) case. This suggests that the control inputs are less coupled with the tILC strategy proposed in this work.

5.2.2 6-DOF (soft arm) : In this case, the desired link trajectory goes from $q(0) = [0, 0, 0, 0, 0, 0]^T$deg to $q(t_\text{f}/2) = [60, -10, -45, -25, -90, -45]^T$deg and then goes back to the initial position, in $t_\text{f} = 20$s . As in the simpler 2-DOF case, the reference trajectory is a five order minimum jerk trajectory and the stiffness regulation parameters are set as $\theta_{\text{sr},j} = 0.2\Delta_{\text{m},j}$ for the soft case and $\theta_{\text{sr},j} = 0.8\Delta_{\text{m},j}$ for the stiff case, where $\Delta_{\text{m},j}$ is the maximum s.r.p. for the *j*-th actuator ($j = 1, ...6$). For both ILC approaches the control parameter is chosen as $R = 9$.

Results: Fig. 9 shows the evolution of e^k for either position (dashed blue line) and torque (solid orange line) ILC case for the soft to stiff transition (Fig. 9a) and the stiff to soft transition (Fig. 9b), while numerical results are reported in Table 3. For these cases, 40 iterations are required to reach a small tracking error either in soft and in stiff behaviors (left-side curves of both plots in Fig. 9a and Fig. 9b). At the $41st$ iteration the s.r.p. is changed and other 40 iterations are performed (right-side of the plots in Fig. 9a and Fig. 9b). For the proposed strategy (tILC) the trajectory tracking at each joint is reported in Fig. 10 and Fig. 11 for the soft to stiff and stiff to soft transition, respectively. In the figures we show six meaningful iterations, i.e., $k = \{1, 20, 40, 41, 60, 80\}$. The reference trajectory is depicted with a dashed black line. Fig. 9a and Fig. 9b show that for this complex structure, the differences of the gaps between the errors e^{40} (FF40) and e^{41} (FF40+1) are more visible. Indeed, the ratio between the error gap in the tILC and the error gap in the pILC case is: 0.16 for the soft to stiff transition and 0.18 for the stiff to

[‖] Please note that metric (63) is averaged between the joints to simplify the performance comparison between structures with a different number of joints. Furthermore, it is normalized w.r.t. the terminal time to simplify the performance comparison between different trajectories.

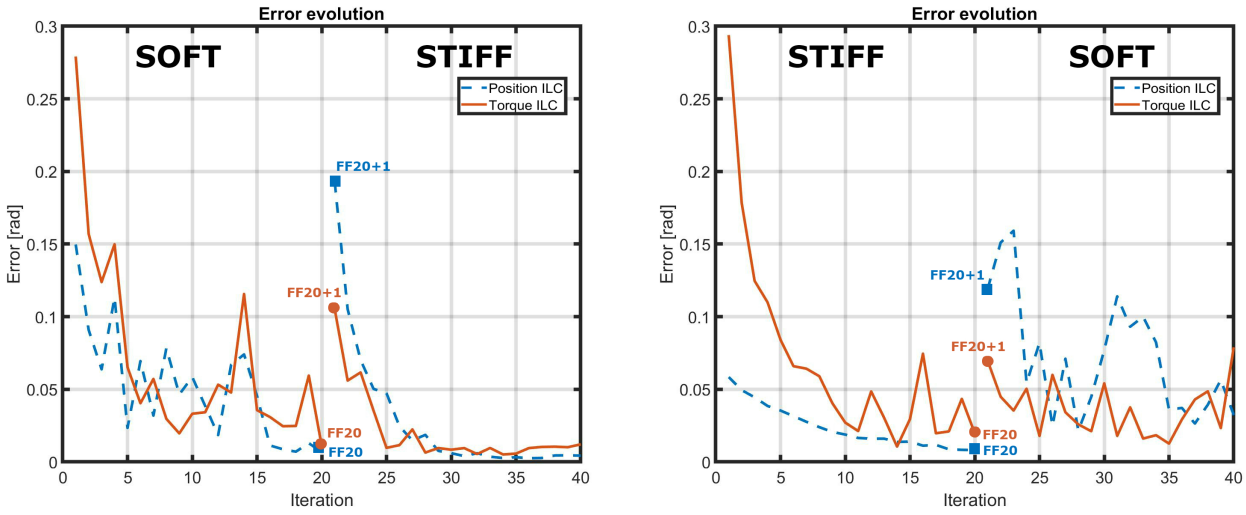

(a) Soft to Stiff transition **(b)** Stiff to Soft transition

Figure 8. Evolution of the error e^k over iterations for the *2*-DOF structure. The results for the soft to stiff and stiff to soft transitions are depicted in (a) and (b), respectively. Both the position (dashed blue line) and torque (solid orange line) ILC approaches are reported. The figures show the convergences of the error during the first 20 iterations (lef-side of plots in (a) and (b)) and the convergences after s.r.p. change (right-side of the plots). FF20 is the error at the 20th iteration e^{20}, and FF20+1 is the same error at the first iteration after s.r.p. change e^{21}. The error gaps in (a) are: $gap_P = 0.186$rad and $gap_T = 0.094$rad, and in (b) are: $gap_P = 0.111$rad and and $gap_T = 0.050$rad, where the pedices denote, P position and T torque ILC case.

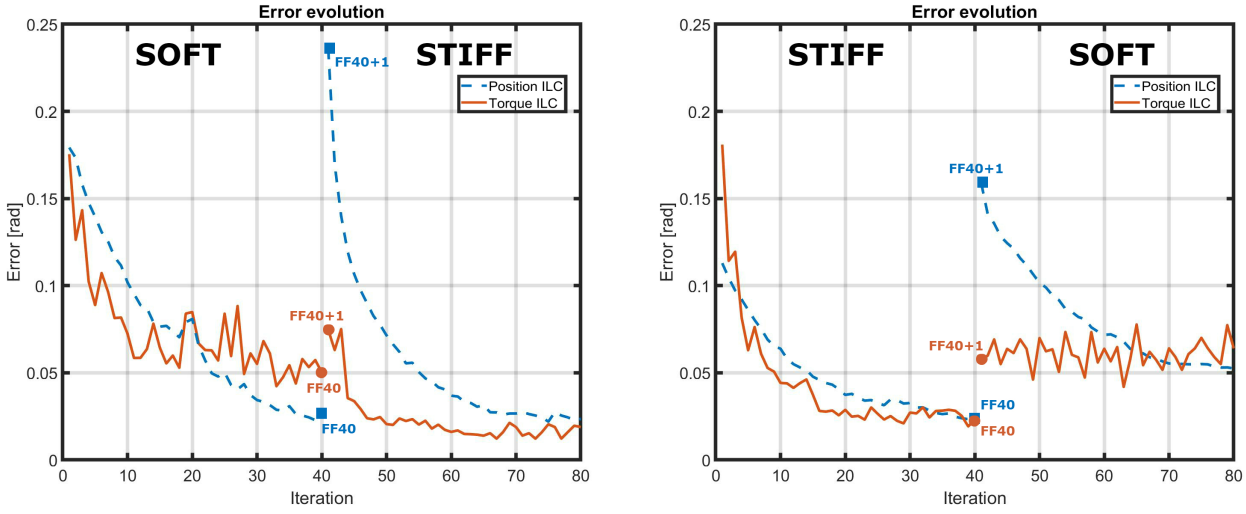

(a) Soft to Stiff transition **(b)** Stiff to Soft transition

Figure 9. Evolution of the error e^k over iterations for the *6*-DOF robotic arm. The results for the soft to stiff and stiff to soft transitions are depicted in (a) and (b), respectively. Both the position (dashed blue line) and torque (solid orange line) ILC approaches are reported. The figures show the convergences of the error during the first 40 iterations (lef-side of plots in (a) and (b)) and the convergences after s.r.p. change (right-side of the plots). FF40 is the error at the 40th iteration e^{40}, and FF40+1 is the same error at the first iteration after s.r.p. change e^{41}. The error gaps in (a) are: $gap_P = 0.208$rad and $gap_T = 0.034$rad, and in (b) are: $gap_P = 0.134$rad and $gap_T = 0.024$rad where the pedices denote, P position and T torque ILC case, respectively. The figures show that for this complex structure, the comparison from error gaps in (a) and (b) is even more visible.

soft transition. For the soft to stiff transition the gaps ratio can be also graphically evaluated from the frame sequences shown in Fig. 1 and in Fig. 12. The same results can also be seen in Extension 1. Similar to the previous case, these results validate the proposed control strategy and allow us to conclude that the decoupling is verified even in robots with a higher number of joints.

5.2.3 Discussion: Similarly to the pILC strategy, the iterative process of the tILC method converges, and allows us to achieve good tracking performance in all scenarios. This result can be retrieved from Fig. 8 and Fig. 9, and also from Table 2 and Table 3, by comparing the tracking error at the first iteration e^1 with the error at the $20th$ iteration e^{20} (for the 2-DOF case) or the error at the $40th$ iteration e^{40} (for the 6-DOF case). The learning convergence can be also noticed by comparing the trajectory tracking at the first iteration

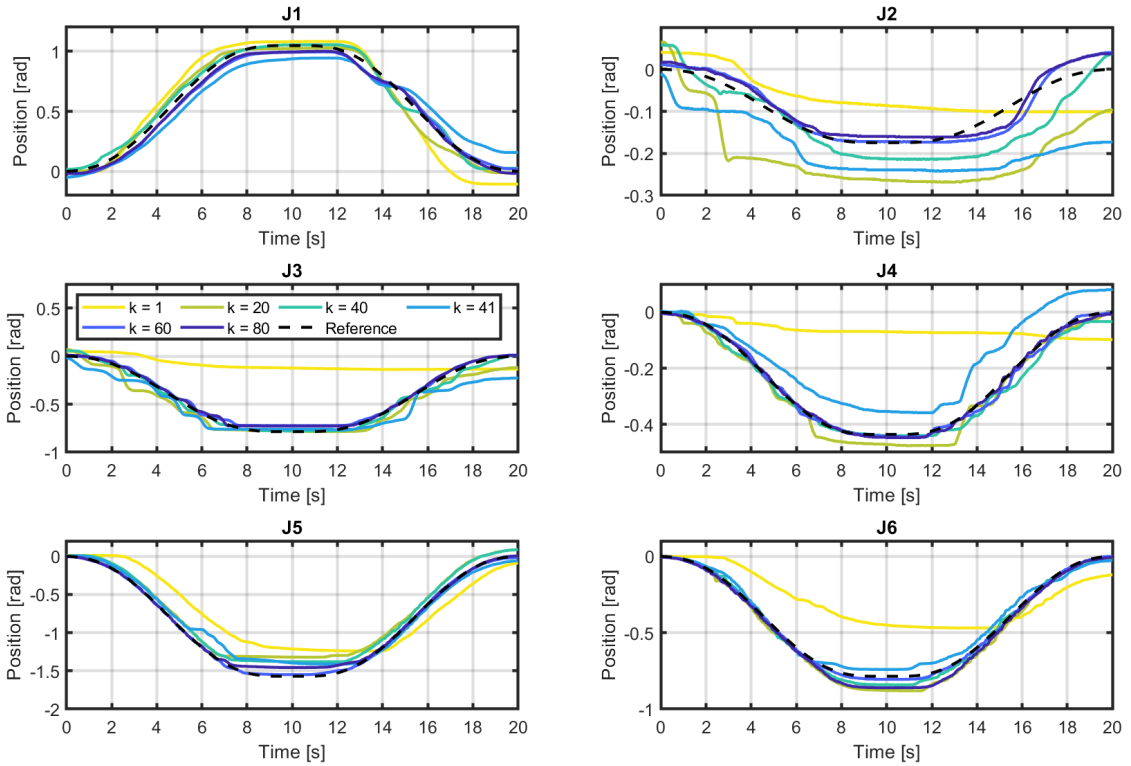

Figure 10. Joint trajectory tracking for the tILC method: soft to stiff transition. Six of the iterations performed are reported: from $k = 1$ to $k = 80$. Among them, the first three lines, i.e. $k = \{1, 20, 40\}$, are performed with a soft behavior, while the last three, $k = \{41, 60, 80\}$, are obtained with a stiff behavior. The dashed black line is the reference trajectory for each joint. The learning improvement can be verified by comparing $k = 1$ with $k = 40$, while the motion/stiffness decoupling by comparing $k = 40$ and $k = 41$. The joint $J2$ is the more subjected to the friction effect, especially in the soft case.

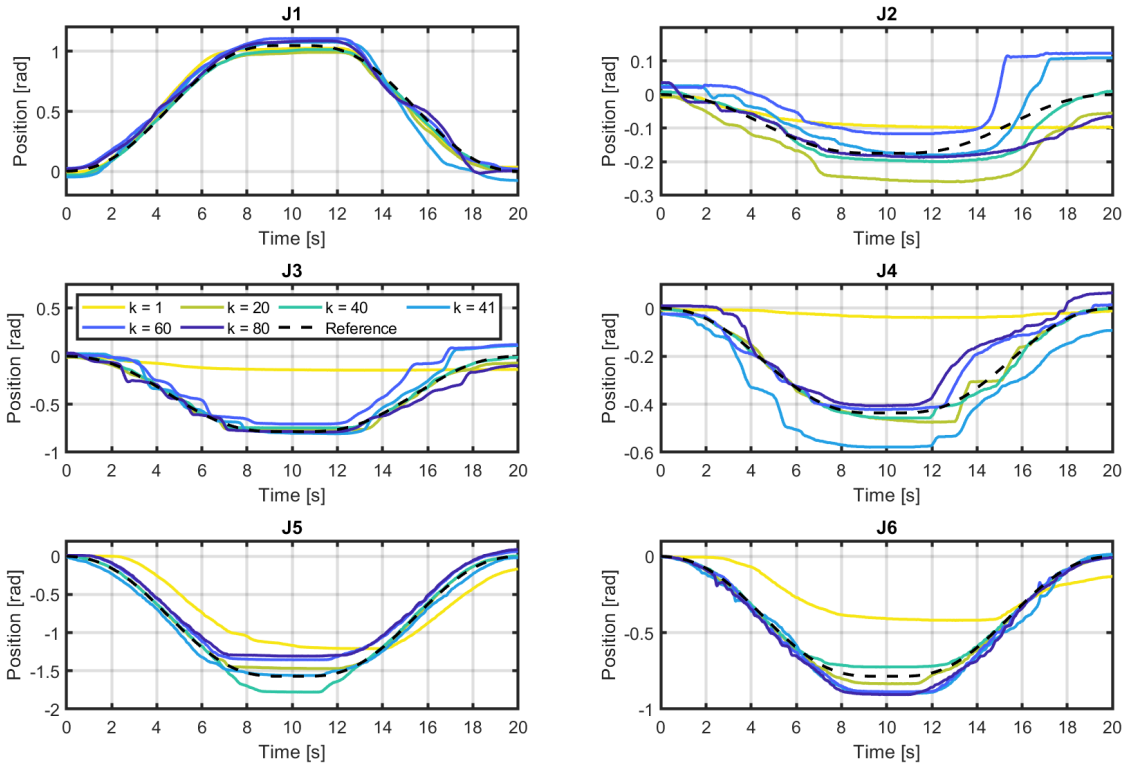

Figure 11. Joint trajectory tracking for the tILC method: stiff to soft transition. Six of the iterations performed are reported: from $k = 1$ to $k = 80$. Among them, the first three lines, i.e. $k = \{1, 20, 40\}$, are performed with a stiff behavior, while the last three, $k = \{41, 60, 80\}$, are obtained with a soft behavior. The dashed black line is the reference trajectory for each joint. The learning improvement can be verified by comparing $k = 1$ with $k = 40$, while the motion/stiffness decoupling by comparing $k = 40$ and $k = 41$. The joint $J2$ is the more subjected to the friction effect, especially in the soft case.

($k = 1$) and at the $40th$ iteration ($k = 40$) in Fig. 10 and Fig. 11. However, it is worth saying that, in terms of tracking error, the error of tILC is slightly larger than the pILC one, especially in the soft case. This first part of the experiment (i.e. the learning process) shows the effectiveness of the tILC method in tracking the desired trajectory. Instead, the second part aims to prove the motion/stiffness decoupling. Indeed, iteration $k = 41$ shows the performance degradation after a change in the stiffness of the system. The results show that, as soon as this change occurs, the error gaps caused by a stiffness change are considerably smaller in the tILC case w.r.t. the pILC case. This can be numerically verified from Table 2 and Table 3 by comparing the errors e^{20} and e^{21} for the 2-DOF structure, and similarly for the 6-DOF arm (cf. e^{40} and e^{41}).

In terms of individual joint performance, Table 4 shows the integral absolute error of each joint at the iteration $k = \{1, 40, 41, 80\}$, for the tILC case of the 6-DOF arm. From Table 4 it is possible to see that also the error at each joint converges during the first 40 iterations. In addition, the trajectory tracking for each joint is reported in Fig. 10 and Fig. 11, and in the video attachment (Extension 1). From these figures we can conclude that, especially in soft behavior, the worse tracking performance is given by the second joint J2. This is mainly due to the presence, in our experimental setup, of a gravity compensation mechanism composed of a pair of springs, belts and several pulleys (more details in Appendix D). These components are more subjected to wear phenomena and friction, that in turn affect joint J2 and J3. The mechanism also couples the two joints J2 and J3. Furthermore, due to the mechanical structure of the manipulator, we have that the torque seen at the joint J4 is more influenced by the trajectory we impose to the last two joints (i.e. J5, J6). This influence is also caused by the weight of the last components of the arm that affects J4, differently to what happens to J2 and J3, for which the gravity is compensated.

Besides these positive results, the experiments also highlight the sensitivity of the tILC method to undesired friction effects on both the test-beds. Indeed, as discussed in Section 4.3, these effects change for each iteration, thus they can not be completely learned. In addition, these effects may depend on the value of θ_{sr}, resulting in a more visible influence with soft behavior than with stiff behavior, for both the controllers. The reader can observe this phenomenon in Fig. 8 and Fig. 9, where fluctuations of the error can be noticed.

On the other hand, pILC presents fewer irregularities in the convergence, due to the loop closed in position, that allows compensating the friction phenomena. It is reasonable to conclude that, whenever the system is affected by friction effects, and the task does not require to change the stiffness profile, tILC does not present clear advantages compared to pILC. Conversely, if the stiffness profile of the task must be changed considerably, then tILC should be chosen, taking into account the friction effect. In order to reduce the performance degradation due to friction, high-gain feedback could be employed, however, this would counteract the goal of this work regarding the stiffness preservation (discussed in Section 2).

The recovery part of the experiment shows that for the soft to stiff transition, tILC requires few more iterations to regain performances after the stiffness change. It is worth noting that the number of iterations that tILC requires to regain performance is less if compared with the pILC case. Indeed, the latter method requires an entirely new learning process, as shown in Fig. 8a and Fig. 9a. Differently, in the stiff to soft transition, tILC performs much better in terms of the error gaps achieved after the change of stiffness. Indeed, for this case, after the stiffness change, the tracking error reaches immediately the best value achievable by the compliant structure. Then, no more iterations are needed to regain performance (differently from the pILC, Fig. 9b).

From a comparative point of view, tILC improves the results of the pILC, meaning that it allows to generalize the learning process w.r.t. possible change of the compliant behavior of the system. Despite this, dealing with a control strategy based on torque, the results are more sensitive to friction effects. This may restrict the effectiveness of the tILC method to all the cases in which such effects are negligible. Also, other sources of error compromising the effectiveness of tILC may depend on the characteristics of the system itself. For instance, if the actuation unit is relocated w.r.t. the variable to be controlled, the interconnecting mechanism (e.g., a Bowden cable (Zhang et al. 2017)) can be subjected to vibrations, thermal variability or in general will be more prone to friction. For this reason, to improve the performance of the tILC method, the use of friction compensation techniques will be investigated in future works.

5.3 Stiffness preservation

This experiment starts with the same learning process of Section 5.2, considering only the tILC case. Once the trajectory is learned, a fixed object is placed along the desired trajectory path. The test is performed with two compliant behaviors changing the s.r.p. θ_{sr}: low value (*soft*) and high value (*stiff*). At a certain time instant (dashed magenta vertical line in Fig. 13 and Fig. 14) the system impacts the

		e^1 [rad]	e^{20} [rad]	e^{21} [rad]	e^{40} [rad]
a)	**pILC**	0.150	0.007	0.193	0.004
	tILC	0.279	0.011	0.105	0.012
b)	**pILC**	0.058	0.008	0.119	0.032
	tILC	0.294	0.020	0.070	0.079

Table 2. Tracking error e^k at the k-th iteration of the two strategies pILC and tILC for the 2-DOF system. The first two rows (a) show the transition from soft to stiff, and the stiff to soft case is shown in the last two rows (b).

		e^1 [rad]	e^{40} [rad]	e^{41} [rad]	e^{80} [rad]
a)	**pILC**	0.179	0.027	0.236	0.023
	tILC	0.175	0.050	0.075	0.019
b)	**pILC**	0.113	0.025	0.159	0.053
	tILC	0.181	0.023	0.057	0.064

Table 3. Tracking error e^k at the k-th iteration of the two strategies pILC and tILC for the 6-DOF system. The first two rows (a) show the transition from soft to stiff, and the stiff to soft case is shown in the last two rows (b).

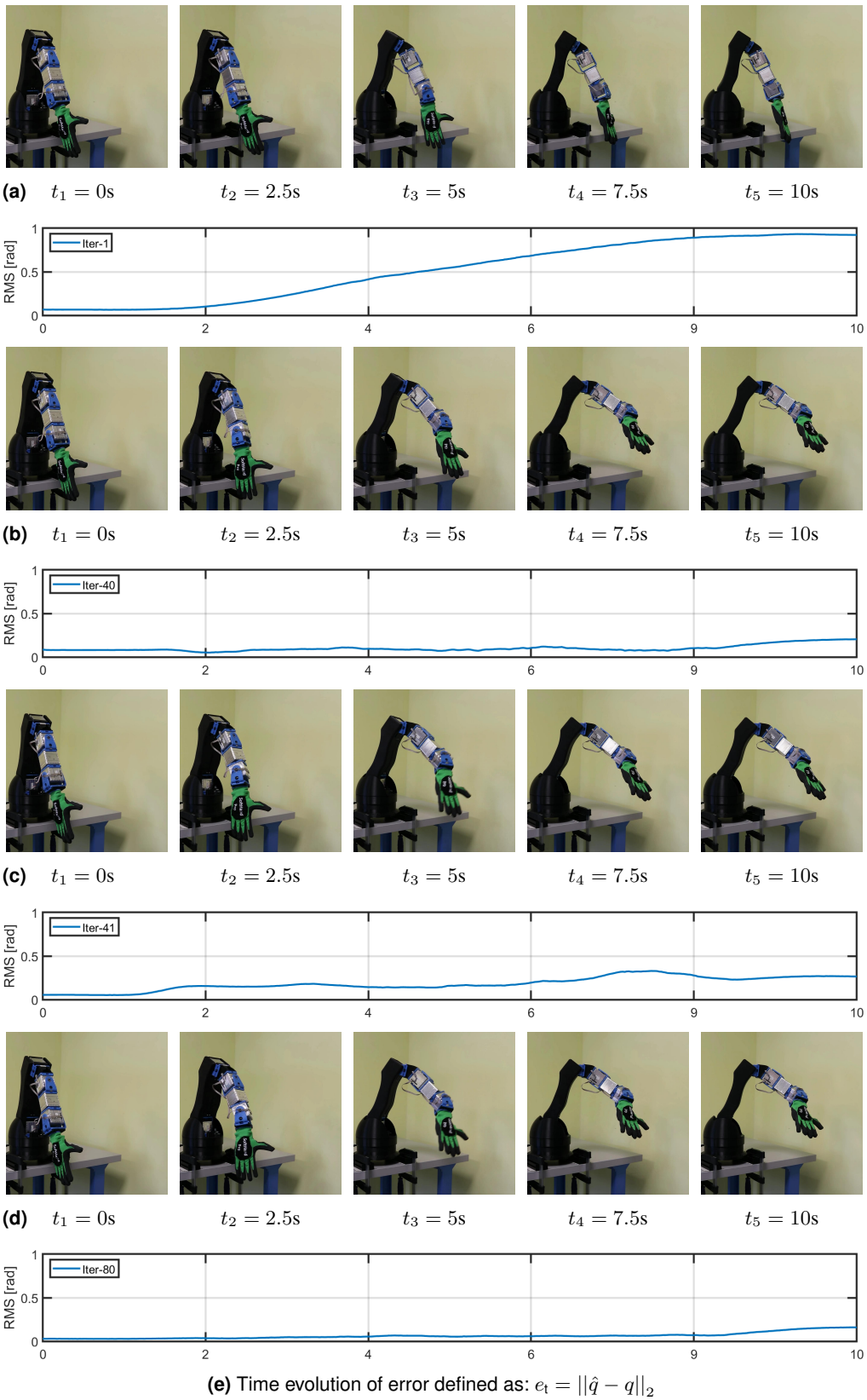

(e) Time evolution of error defined as: $e_{\mathrm{t}} = ||\hat{q} - q||_2$

Figure 12. Frame sequences of the soft-to-stiff experimental task (see also Extension 1). Figures report the frame sequences of the task for the first and last iteration in soft case, (a) and (b), and first and last iteration in stiff case, after stiffness regulation parameter change, (c) and (d). The plots report the time evolution of the Euclidean norm (2-norm) of the joints error as reported in the caption (e), for the four cases respectively.

obstacle. Then, the stiffness is computed as in (92), and it is compared to the obstacle-free stiffness profile.

5.3.1 2-DOF (horizontal configuration) : For this configuration the minimum jerk joint trajectory goes from $q(0) = [0, 0]^T$deg to $q(t_{\mathrm{f}}) = [35, 45]^T$deg in $t_{\mathrm{f}} = 2$s. The stiffness

regulation parameters are set as $\theta_{\mathrm{sr},j} = 0.2\Delta_{\mathrm{m},j}$ for the soft case and $\theta_{\mathrm{sr},j} = 0.8\Delta_{\mathrm{m},j}$ for the stiff case, where $\Delta_{\mathrm{m},j}$ is the maximum deflection reachable from the j-th actuator ($j = 1, 2$). The ILC control parameter is chosen as $R = 5$.

Results: Fig. 13 shows the stiffness profiles, computed as in (92), in case of obstacle impact (solid blue lines) and obstacle-free execution (dashed red lines). From the figures it is possible to conclude that, either with the soft (Fig. 13a) as with the stiff (Fig. 13b) behavior, the stiffness is preserved at the moment of impact. With this particular configuration the system is not altered by external load. Thus, in the obstacle-free case, the stiffness remains constantly at the desired value during all the execution.

5.3.2 2-DOF (vertical configuration) : For this configuration the minimum jerk joint trajectory goes from $q(0) = [0, 0]^T$deg to $q(t_\mathrm{f}) = [35, 45]^T$deg in $t_\mathrm{f} = 2$s. The stiffness regulation parameters are set as $\theta_{\mathrm{sr},j} = 0.2\Delta_{\mathrm{m},j}$ for the soft case and $\theta_{\mathrm{sr},j} = 1\Delta_{\mathrm{m},j}$ for the stiff case, where $\Delta_{\mathrm{m},j}$ is the maximum deflection reachable from the j-th actuator ($j = 1, 2$). Note that, for the sake of visibility, the stiffness regulation parameter in the stiff case is higher w.r.t. the one used in the horizontal case. The ILC control parameter is chosen as $R = 5$.

Results: Fig. 14 shows the stiffness profiles, computed as in (92), in case of obstacle impact (solid blue lines) and obstacle-free execution (dashed red lines). As in the horizontal configuration, the figures suggest that, either with the soft (Fig. 14a) or with the stiff (Fig. 14b) behavior, the stiffness is preserved at the moment of impact. However, the external load (i.e., gravity action) is not negligible and alters the stiffness profiles, as visible in the soft case. This causes an increment of the stiffness values even in the obstacle-free execution.

5.4 Application:

One practical example where it is useful to apply the tILC strategy proposed in this work, is the button-pushing task reported in Mengacci et al. (2019). In this example, the task requires to interact with a switch button, with the goal of correctly push it. Moreover, as discussed in the referenced paper, the task can not be performed with a low compliant behavior, due to interaction stability issues. Thus, to reach the button it is important to perform a good trajectory tracking and to push the button a specific stiffness is required. Furthermore, a compliant behavior can still be needed to prevent any damage to the environment or to the manipulator itself during the interaction.

Thus, by exploiting the proposed scheme, the control action that leads to a satisfactory trajectory tracking can be firstly learned with any compliant (soft) behavior. Once this control action is successfully learned, the compliant behavior can be changed to meet the task requirements, i.e., in this case, to push the button without slipping. Then, for this case, and for other cases of trajectory tracking for elastic robots with variable compliance, the iterative procedure is considerably reduced if the presented control strategy is adopted.

	tILC	e^1 [rad]	e^{40} [rad]	e^{41} [rad]	e^{80} [rad]
a)	J1	0.094	0.028	0.084	0.023
	J2	0.148	0.084	0.085	0.014
	J3	0.205	0.062	0.084	0.014
	J4	0.184	0.017	0.077	0.005
	J5	0.234	0.093	0.085	0.032
	J6	0.188	0.017	0.034	0.026
b)	J1	0.142	0.016	0.074	0.032
	J2	0.052	0.028	0.034	0.062
	J3	0.222	0.014	0.052	0.068
	J4	0.203	0.008	0.083	0.042
	J5	0.266	0.051	0.045	0.124
	J6	0.200	0.020	0.055	0.048

Table 4. Integral absolute error at the k-th iteration of the tILC strategy for each joint of the 6-DOF system. The first six rows (a) show the transition from soft to stiff, while the stiff to soft case is shown in the last six rows (b).

6 Conclusions

In this paper, a novel control scheme has been presented with the aim to track a desired link position trajectory without compromising the natural compliant behavior of an articulated soft robot. We proved that, under the assumptions of strong elastic coupling and homogeneity, the dynamics of a robot with lumped elasticity at the joints can be decoupled into two separate parts, one representing the dynamics of a flexible joint robot and the other one that allows the stiffness adjusting. Then, a torque-based ILC approach was proposed to control the link position and a PI control loop was implemented to track the stiffness regulation parameter.

Combining these two actions, the overall control strategy results in a model-free decoupled torque control scheme useful for driving robotic systems equipped with compliant actuators. In addition, the general formulation of this method allows to apply this scheme to most VSAs presented in the literature.

We discussed what are the main points to be considered whenever the theoretical control strategy has to be implemented in real applications. We analyzed the consequences of a lack of validity of some of the hypotheses and we proposed some solutions. Then, experimental validation of the strategy on symmetric A-A VSAs has been done proving that the proposed method effectively reduces the coupling between the learned control action and the stiffness selection. This is verified either for a simple *1*-DOF or *2*-DOF structures and a more complex *6*-DOF arm. Impact tests proved also that the stiffness was preserved during the tasks.

To summarize, in this work we showed that the proposed tILC scheme allows us to track a given position trajectory independently from the stiffness profile. Furthermore, it is possible to learn the control action, needed to perform accurate positioning of the system, in a safe condition (i.e., with low stiffness profile) either for the surrounding environment or for the structure itself. Once learned, the same control action can be used with different compliant behavior to adapt to the task requirements. This control strategy finds direct application on tasks in which intentional, or unexpected, interactions with the environment may occur, e.g., the button-pushing task presented in Section 5.4.

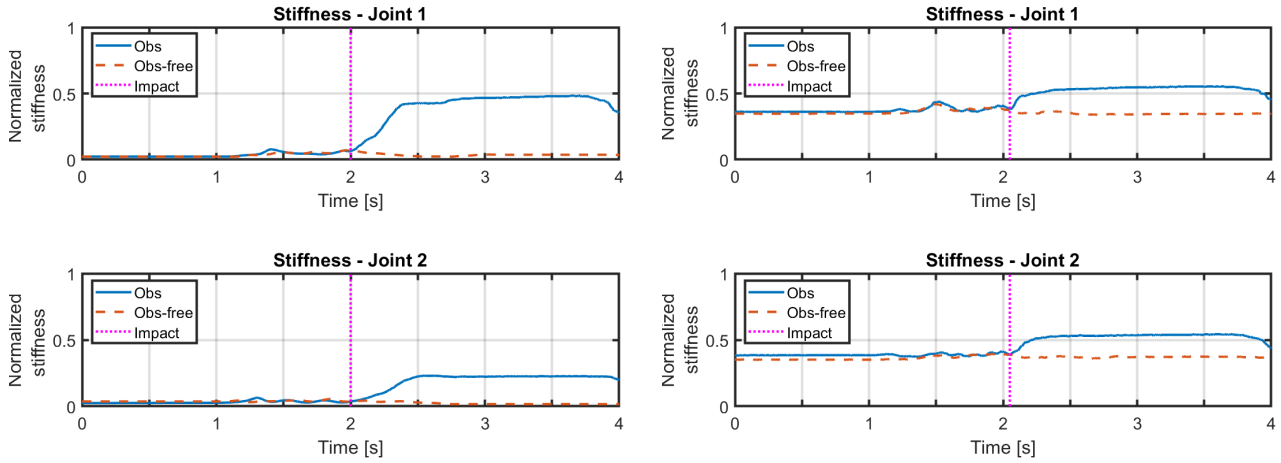

(a) Soft case **(b)** Stiff case

Figure 13. Normalized joints stiffness for the *2*-DOF horizontal structure. In figures are reported the joints stiffness in the soft case (a) and in the stiff case (b), computed as in (92) and normalized by the maximum stiffness of the respective actuator. The moment of impact is marked with a dotted magenta vertical line. The stiffness profile in case of obstacle impact is decited in solid blue lines, while the obstacle-free execution is depicted in dashed red lines. For this configuration, the two profiles are identical before the impact, while after the collision a gap grows.

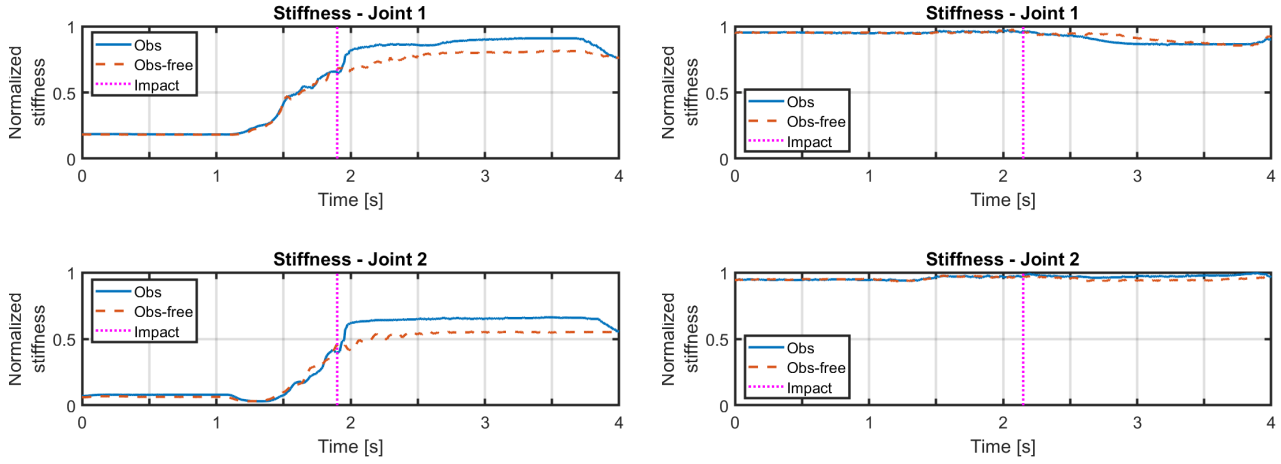

(a) Soft case **(b)** Stiff case

Figure 14. Normalized joints stiffness for the *2*-DOF vertical structure. In figures are reported the joints stiffness, in the soft case (a) and in the stiff case (b), computed as in (92) and normalized by the maximum stiffness of the respective actuator. The moment of impact is marked with a dotted magenta vertical line. The stiffness profile in case of obstacle impact is depicted in blue solid line, while the obstacle-free execution is depicted in dashed red line. Even in this case the two profiles are identical before the impact. However, for this setup, the gravitational contribute is not negligible and alters the stiffness of the system. This can be seen expecially in the soft case in (a).

The experiments carried out in this work showed that the main limitation of the proposed method resides in the presence of friction. Indeed, friction plays a crucial role in the tracking error achieved and for the motion/stiffness decoupling. The frictional effects are also strongly related to the actuation employed in the experiments. This is the case of our experimental setup that, especially when operating with low stiffness, showed high sensitivity to friction, leading to a significant error on the trajectory tracking for some joints. It is also worth noting that the individual errors at the joints affect the resulting Cartesian position (cf. video attachment in Extension 1), depending also on the kinematic structure and the number of degrees of freedom of the system.

For all these reasons, to overcome the practical limitations of the method and to further improve the tracking performance, future works will be devoted to limit the friction influence. To achieve this goal, both improvements of the hardware and friction compensation techniques will be investigated.

Acknowledgements

The authors would like to thank Riccardo Persichini for the work done in designing and building the 6-DOF manipulator and qbrobotics company for providing the required hardware.

Funding

The present work has received funding from the European Unions Horizon 2020 Research and Innovation Programme under Grant Agreement No. 780883 (THING), No. 732737 (ILIAD).

Appendix A. Index to multimedia extensions

Table of Multimedia Extensions

Extension	Media type	Description
1	Video	Demonstration of Experiment 1 for the 6-DOF arm

Appendix B. Derivation of A, B, C matrices

In this Appendix we derive the matrices A, B and C shown in Proposition 1 of Section 4.

From Assumption 1, we write

$$\frac{\partial V_i}{\partial q_j} = \frac{\partial f_i}{\partial y_i}\frac{\partial y_i}{\partial q_j} g_i, \quad \forall i = 1,..s,\ \forall j = 1,..n, \tag{64}$$

thus,

$$\frac{\partial V^T}{\partial q} = \begin{bmatrix} \sum_i \frac{\partial V_i}{\partial q_1} \\ \vdots \\ \sum_i \frac{\partial V_i}{\partial q_n} \end{bmatrix} = \begin{bmatrix} \frac{\partial y_1}{\partial q_1} & \cdots & \frac{\partial y_s}{\partial q_1} \\ & \vdots & \\ \frac{\partial y_1}{\partial q_n} & \cdots & \frac{\partial y_s}{\partial q_n} \end{bmatrix} \overbrace{\begin{bmatrix} \frac{\partial f_1}{\partial y_1} g_1 \\ \vdots \\ \frac{\partial f_r}{\partial y_s} g_s \end{bmatrix}}^{z}, \tag{65}$$

where $z \in \mathbb{R}^{s\times 1}$. From (14), $\frac{\partial y_i}{\partial q} = a_i^T$, hence

$$\frac{\partial V^T}{\partial q} = \underbrace{\begin{bmatrix} a_1^T & \cdots & a_s^T \end{bmatrix}}_{A} z, \tag{66}$$

with $A \in \{-1, 0, 1\}^{n\times s}$.

We suppose here, without loss of generality**, that the vector θ is reordered such that

$$\begin{aligned} \theta &= \begin{bmatrix} \theta_{\mathrm{d}}^T & \theta_{\mathrm{a}}^T \end{bmatrix}^T \\ &= \begin{bmatrix} \theta_{\mathrm{d},1} & \cdots & \theta_{\mathrm{d},r} & \theta_{\mathrm{a},(r+1)} & \cdots & \theta_{\mathrm{a},(m-r)} \end{bmatrix}^T. \end{aligned} \tag{67}$$

The partial derivative w.r.t. the motor positions can be written as

$$\frac{\partial V^T}{\partial \theta} = \begin{bmatrix} \frac{\partial V^T}{\partial \theta_{\mathrm{d}}} \\ \hline \frac{\partial V^T}{\partial \theta_{\mathrm{a}}} \end{bmatrix} = \begin{bmatrix} \sum_i \frac{\partial V_i^T}{\partial \theta_{\mathrm{d}}} \\ \hline \sum_i \frac{\partial V_i^T}{\partial \theta_{\mathrm{a}}} \end{bmatrix}, \tag{68}$$

where

$$\begin{cases} \frac{\partial V_i^T}{\partial \theta_{\mathrm{d}}} = \frac{\partial f_i}{\partial y_i}\frac{\partial y_i^T}{\partial \theta_{\mathrm{d}}} g_i \\ \frac{\partial V_i^T}{\partial \theta_{\mathrm{a}}} = f_i \frac{\partial g_i}{\partial w_i}\frac{\partial w_i}{\partial \theta_{\mathrm{a}}} \end{cases}, \quad \forall i = 1,..s. \tag{69}$$

from which

$$\frac{\partial V^T}{\partial \theta} = \begin{bmatrix} \begin{bmatrix} \frac{\partial y_1^T}{\partial \theta_{\mathrm{d}}} & \cdots & \frac{\partial y_s^T}{\partial \theta_{\mathrm{d}}} \end{bmatrix} \overbrace{\begin{bmatrix} \frac{\partial f_1}{\partial y_1} g_1 \\ \vdots \\ \frac{\partial f_s}{\partial y_s} g_s \end{bmatrix}}^{z} \\ \hline \begin{bmatrix} \frac{\partial w_1^T}{\partial \theta_{\mathrm{a}}} & \cdots & \frac{\partial w_s^T}{\partial \theta_{\mathrm{a}}} \end{bmatrix} \underbrace{\begin{bmatrix} f_1 \frac{\partial g_1}{\partial w_1} \\ \vdots \\ f_s \frac{\partial g_s}{\partial w_s} \end{bmatrix}}_{v} \end{bmatrix}, \tag{70}$$

where $v \in \mathbb{R}^{s\times 1}$. From (14) $\frac{\partial y_i^T}{\partial \theta_{\mathrm{d}}} = b_i^T$, $\frac{\partial w_i^T}{\partial \theta_{\mathrm{a}}} = c_i^T$ and then (70) becomes

$$\frac{\partial V^T}{\partial \theta} = \begin{bmatrix} \overbrace{\begin{bmatrix} b_1^T & \cdots & b_s^T \end{bmatrix}}^{B} z \\ \hline \underbrace{\begin{bmatrix} c_1^T & \cdots & c_s^T \end{bmatrix}}_{C} v \end{bmatrix}, \tag{71}$$

with $B \in \{-1, 0, 1\}^{r\times s}$ and $C \in \{-1, 0, 1\}^{(m-r)\times s}$.

Thus (66) and (71) lead to

$$\frac{\partial V(q,\theta)^T}{\partial q} = A \cdot z(q,\theta), \tag{72}$$

$$\frac{\partial V(q,\theta)^T}{\partial \theta} = \begin{bmatrix} B \cdot z(q,\theta) \\ \hline C \cdot v(q,\theta) \end{bmatrix}. \tag{73}$$

Appendix C. Elastic models

In the following we report the evaluation of the matrices A, B and Γ for some examples of compliant actuators found in literature.

Series Elastic Actuator (SEA)

For completeness we report here also the case of an actuator in which the output link is connected to only one motor ($m = n = 1$) through a spring element with fixed elasticity (K_1). Note that, for this model, Proposition 2 can not be applied since the stiffness can not be varied. The elastic potential can be written as

$$V(q,\theta) = \frac{K_1}{2}(q-\theta)^2. \tag{74}$$

The partial derivative w.r.t. the output link is

$$\frac{\partial V(q,\theta)}{\partial q} = K_1(q-\theta), \tag{75}$$

while the partial derivative w.r.t. the motor position is

$$\frac{\partial V(q,\theta)}{\partial \theta} = -K_1(q-\theta). \tag{76}$$

From (75) and (76) it is possible to show that the matrices are $A = 1,\ B = -1,\ \Gamma = -1$. The deflecting motor is $\theta_{\mathrm{d}} = \theta$ and there is no adjusting motor.

**Note that reordering the motor vector can always be done since the motors dynamics are decoupled (i.e. J and D are diagonal matrices).

Adjustable Variable Stiffness Actuator (AwAS)

This actuator, proposed in Jafari et al. (2013), implements the variable lever arm principle in which, to vary the stiffness of the output link, the spring point is changed. For this design two different motors are used to drive the joint and to adjust the stiffness, separately, i.e., $m = 2, r = 1$. The elastic potential can be written as

$$V(q,\theta) = \frac{K_s}{2}\left[(l_0 + \theta_2 \sin(q-\theta_1))^2 + \right. \\ \left. + (l_0 - \theta_2 \sin(q-\theta_1))^2\right]. \quad (77)$$

The partial derivative w.r.t. the output link is

$$\frac{\partial V(q,\theta)}{\partial q} = \frac{K_s}{2}\left[2\theta_2 \cos(q-\theta_1)(l_0 + \theta_2 \sin(q-\theta_1))^2 + \right. \\ \left. - 2\theta_2 \cos(q-\theta_1)(l_0 - \theta_2 \sin(q-\theta_1))^2\right], \quad (78)$$

while the partial derivatives w.r.t. the motor positions are

$$\frac{\partial V(q,\theta)}{\partial \theta_1} = -\frac{K_s}{2}\left[2\theta_2 \cos(q-\theta_1)(l_0 + \theta_2 \sin(q-\theta_1))^2 + \right. \\ \left. - 2\theta_2 \cos(q-\theta_1)(l_0 - \theta_2 \sin(q-\theta_1))^2\right], \quad (79)$$

$$\frac{\partial V(q,\theta)}{\partial \theta_2} = \frac{K_s}{2}\left[2 \sin(q-\theta_1)(l_0 + \theta_2 \sin(q-\theta_1))^2 + \right. \\ \left. - 2 \sin(q-\theta_1)(l_0 - \theta_2 \sin(q-\theta_1))^2\right]. \quad (80)$$

From (78), (79) and (80) it is possible to show that the matrices are $A = [1 \;\; 0]$, $B = \begin{bmatrix} -1 & 0 \\ 0 & 0 \end{bmatrix}$ and $\Gamma = [-1 \; 0]$, given the motors partitioning with $\theta_d = \theta_1$ and $\theta_a = \theta_2$.

vsaUT (II)

As for the previous case, the VSA proposed in Visser et al. (2011) is based on a lever arm principle. However, in this case the stiffness is changed by moving the point of application of the force on the lever. Even for this actuator two different motors ($m = 2, r = 1$) allow to change the position and the stiffness. The elastic potential and its derivatives are computed as

$$V(q,\theta) = \frac{1}{2}\frac{(L-\theta_2)^2}{\theta_2^2} K L^2 \sin^2(q-\theta_1), \quad (81)$$

$$\frac{\partial V(q,\theta)}{\partial q} = \frac{K L^2 \cos(q-\theta_1)\sin(q-\theta_1)(L-\theta_2)^2}{\theta_2^2}, \quad (82)$$

$$\frac{\partial V(q,\theta)}{\partial \theta_1} = -\frac{K L^2 \cos(q-\theta_1)\sin(q-\theta_1)(L-\theta_2)^2}{\theta_2^2}, \quad (83)$$

$$\frac{\partial V(q,\theta)}{\partial \theta_2} = -\frac{K L^2 \sin(q-\theta_1)^2(2L-2\theta_2)}{2\theta_2^2} + \\ - \frac{K L^2 \sin(q-\theta_1)^2(L-\theta_2)^2}{\theta_2^3}. \quad (84)$$

From (82), (83) and (84) we obtain that the matrix is given by $A = [1 \;\; 0]$, $B = \begin{bmatrix} -1 & 0 \\ 0 & 0 \end{bmatrix}$ and $\Gamma = [-1 \; 0]$. Even in this case, given the motors partitioning with $\theta_d = \theta_1$ and $\theta_a = \theta_2$.

VSA-Cube

The actuator proposed in Catalano et al. (2011), is of the antagonistic springs with antagonistic motors category. This implies that the motors ($m = 2, r = 2$ in this case) are connected through an elastic element to the output link. Thus, to change the stiffness both motors have to move in opposite direction, while a movement on the same direction changes the equilibrium point. The elastic potential is

$$V(q,\theta) = \frac{k\left((\cosh(a(q-\theta_1)) - 1) +)\right)}{a} + \\ + \frac{k\left((\cosh(a(q-\theta_2)) - 1)\right))}{a}. \quad (85)$$

Note that, for the sake of simplicity, we considered a symmetric agonistic-antagonistic mechanism, i.e., same k and a parameters. The partial derivatives w.r.t. the link and the motors are

$$\frac{\partial V(q,\theta)}{\partial q} = k\left[\sinh(a(q-\theta_1)) + \sinh(a(q-\theta_2))\right], \quad (86)$$

$$\frac{\partial V(q,\theta)}{\partial \theta_1} = -k \sinh(a(q-\theta_1)), \quad (87)$$

$$\frac{\partial V(q,\theta)}{\partial \theta_2} = -k \sinh(a(q-\theta_2)). \quad (88)$$

In this case, from (86), (87) and (88) the matrices are obtained as $A = [1 \;\; 1]$, $B = \begin{bmatrix} -1 & 0 \\ 0 & -1 \end{bmatrix}$ and $\Gamma = [-1 \; -1]$. Differently, here both the motors are deflecting motors thus, $\theta_d = [\theta_1 \;\; \theta_2]^T$ and there is no adjusting motor.

Appendix D. The *6*-DOF VSAs soft arm

In this section we report the mechanical design of the *6*-DOF robotic arm used as experimental setup (Fig. 1). The overall CAD assembly and its main components are illustrated in Fig. 15.

Kinematic analysis

To analyze the direct kinematics of the *6*-DOF arm the standard Denavit-Hartenberg (DH) parameterization was used. The manipulator has a serial, fully actuated, six degrees of freedom structure. The detailed DH table is reported in Tab. 5. To perform manipulation tasks a Pisa/IIT SoftHand (Della Santina et al. 2017b) is mounted as end-effector (ee) of the robotic arm, (element B in Fig. 15). The structural parameters of the manipulator are the following: $l_0 = 0.033$m, $l_1 = 0.077$m, $l_2 = 0.300$m, $l_3 = 0.128$m, $l_4 = 0.089$m, $l_5 = 0.077$m, $l_6 = 0.157$m, $\alpha = 16.4$deg, $\beta = 30$deg, $\gamma = 13.6$deg, $\psi = 18$deg.

Gravity compensation

The overall weight of the *6*-DOF manipulator is approximately 4kg. To improve the payload capabilities of the system, a gravity compensation system has been introduced in the design of the soft arm. The mechanism is depicted in Fig. 16. The key idea is to mechanically remove, through an elastic system, the structure load on the second (J2, Fig. 16a) and third (J3, Fig. 16b) joint. In this way, all the joints can exploit full torque and stiffness range.

	d	θ	a	α
S0-S1	l_0	0	0	0
S1-S2	l_1	q_1	0	$\pi/2$
S2-S3	0	$q_2+\gamma+\pi/2$	l_2	0
S3-S4	0	$q_3+\beta+\alpha+\pi/2$	$l_3\cos(\psi)$	$\pi/2$
S4-S5	$l_3\sin(\psi)$	$q_4+\pi/2$	0	$\pi/2$
S5-S6	l_4+l_5	$q_5+\pi/2$	0	$\pi/2$
S6-S7	0	$q_6+\pi/2$	l_6	$-\pi/2$
S7-See	0	$-\pi/2$	0	0

Table 5. Denavit-Hartenberg table of the *6*-DOF antrophomorphic arm.

Nominal torque	6 Nm
Nominal speed	10 rad/s
Stiffness range	$0.6-30$ Nm/rad
Rotation range	±180 deg
Sensors	position, current
Weight	≈ 0.5 kg

Table 6. Main feautures of qbMove Advanced actuator.

To take into account the elastic system contribution, the potential energy is computed as

$$U_s = \sum_{j=2}^{3} \frac{1}{2} k_j \left(\frac{xp_j + dx_j}{2} \right)^2, \qquad (89)$$

where k_j are the elastic spring constants, xp_j are the pre-tension lengths of the tackles and dx_j are the spring deflections (see Fig. 16c). By the Carnot theorem, the

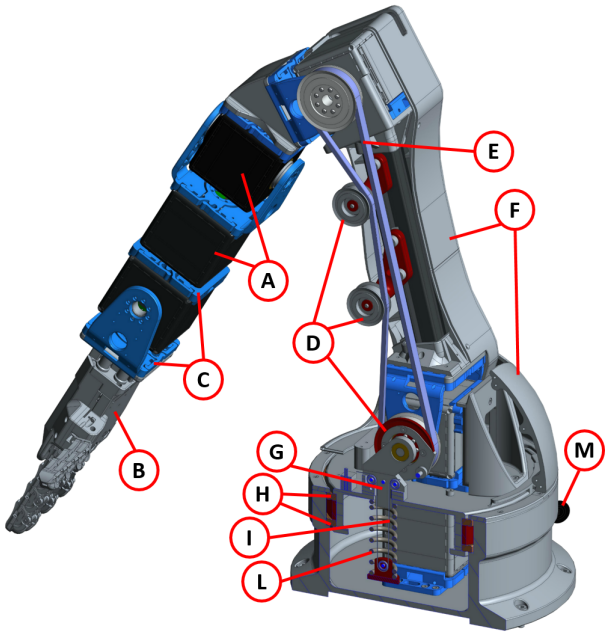

Figure 15. CAD assembly of the *6*-DOF robotic arm with main components highlighted. The components are: **A**) qbMove actuators; **B**) Pisa/IIT SoftHand; **C**) qbMove flanges; **D**) idler (tensioner) pulleys; **E**) Transmission belt; **F**) Plastic covers; **G**) Tackle system; **H**) Base bearings; **I**) Dynema tendon; **L**) Compensation spring; **M**) USB type-B power port.

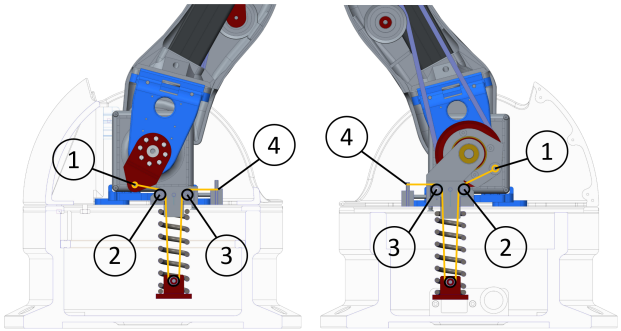

(a) Right view: spring/tendon for J2 compensation. **(b)** Left view: spring/tendon for J3 compensation.

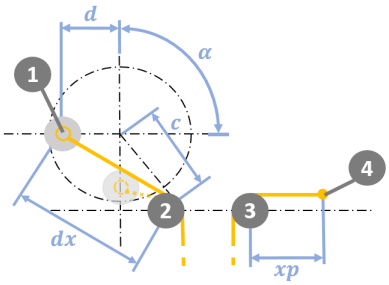

(c) Detail of variables.

Figure 16. Sketch of the gravity compensation mechanisms.

effective spring compression is

$$dx_j = \sqrt{c_j^2 + d_j^2 - 2c_j d_j \cos(\theta_j + \alpha_j)}, \qquad (90)$$

where $\theta_j = \arccos(d_j/c_j)$ are structural angles, c_j, d_j structural parameters and $\alpha_2 = q_2$, $\alpha_3 = \alpha_2 + q_3 + \pi/2 + \gamma$ due to the curvature (γ) of the second link. Note that this mechanism couples the two joints, in fact q_2 angle appears in the computation of dx_3.

Finally, differentiating (89) over joint variables, it is possible to compute the torque contribution of the gravity compensation mechanism as

$$G_s = \frac{\partial U_s}{\partial q}. \qquad (91)$$

Hence, the gravitational term in (1) becomes $G' = G + G_s$ The parameters used in the real mechanism are: $d_2 = 0.024$m, $d_3 = 0.031$m, $xp_2 = 0.011$m, $xp_3 = 0.009$m, $c_2 = 0.036$m, $c_3 = 0.031$m, $k_2 = k_3 = 45$kNm/rad.

Actuation

Each actuation unit consists in a *qbmove Advanced* variable stiffness actuator (Della Santina et al. 2017b), (Catalano et al. 2011). This modular VSA is based on the symmetric antagonistic springs with antagonistic motors variable stiffness mechanism (Vanderborght et al. 2013). Table 6 shows the main features of this device. The data-sheet elastic torque (τ_e) and the stiffness (σ) models are

$$\begin{cases} \tau_e = 2k\cosh(a\theta_{sr})\sinh(a(q-\theta_{eq})) \\ \sigma = 2ak\cosh(a\theta_{sr})\cosh(a(q-\theta_{eq})) \end{cases}, \qquad (92)$$

where $q, \theta_{eq}, \theta_{sr}$ are defined as in Section 4, while $a = 6.7328\text{rad}^{-1}$ and $k = 0.0222$Nm are model parameters.

Note that, due to the prosthaphaeresis simplification (92) appears slightly different from the same model presented in Appendix C.

Electronics and user interfaces

Each actuators has a custom electronic board equipped with a Cypress PSoC 3 micro-controller that allows to drive the two dc motors and to retrieve position signals, from the magnetic encoders (Austria Microsystems AS5045 12-bit resolution), and current signals. The board is programmed with an internal firmware developed in C language. The actuators are mainly used as servo-motors but other control strategies can be implemented into the firmware, e.g., based on position or current measurements. Furthermore, a set of libraries allows to communicate with the internal firmware through common robotic software, such as Matlab/Simulink (www.mathworks.com) or Robot Operating System (ROS) (www.ros.org). Both firmware and libraries (with several examples) are available in the website[††] of the open source Natural Machine Motion Initiative (NMMI) (Della Santina et al. 2017b).

References

Albu-Schäffer A and Bicchi A (2016) Actuators for soft robotics. In: 2nd (ed.) *Handbook of Robotics*, chapter 21. Springer, pp. 508–513.

Albu-Schaffer A, Eiberger O, Grebenstein M, Haddadin S, Ott C, Wimbock T, Wolf S and Hirzinger G (2008) Soft robotics. *IEEE Robotics & Automation Magazine* 15(3).

Albu-Schäffer A and Petit COF (2012) Energy shaping control for a class of underactuated euler-lagrange systems. *IFAC Proceedings Volumes* 45(22): 567–575.

Angelini F, Della Santina C, Garabini M, Bianchi M, Gasparri GM, Grioli G, Catalano MG and Bicchi A (2018) Decentralized trajectory tracking control for soft robots interacting with the environment. *IEEE Transactions on Robotics* .

Bicchi A and Tonietti G (2004) Fast and" soft-arm" tactics [robot arm design]. *IEEE Robotics & Automation Magazine* 11(2): 22–33.

Braun DJ, Howard M and Vijayakumar S (2012) Exploiting variable stiffness in explosive movement tasks. *Robotics: Science and Systems VII* : 25.

Braun DJ, Petit F, Huber F, Haddadin S, Van Der Smagt P, Albu-Schäffer A and Vijayakumar S (2013) Robots driven by compliant actuators: Optimal control under actuation constraints. *IEEE Transactions on Robotics* 29(5): 1085–1101.

Buondonno G and De Luca A (2016) Efficient computation of inverse dynamics and feedback linearization for vsa-based robots. *IEEE Robotics and Automation Letters* 1(2): 908–915.

Catalano MG, Grioli G, Garabini M, Bonomo F, Mancini M, Tsagarakis N and Bicchi A (2011) Vsa-cubebot: A modular variable stiffness platform for multiple degrees of freedom robots. In: *Robotics and Automation (ICRA), 2011 IEEE International Conference on*. IEEE, pp. 5090–5095.

De Luca A (2000) Feedforward/feedback laws for the control of flexible robots. In: *Proceedings 2000 ICRA. Millennium Conference. IEEE International Conference on Robotics and Automation. Symposia Proceedings (Cat. No. 00CH37065)*, volume 1. IEEE, pp. 233–240.

De Luca A and Book WJ (2016) Robots with flexible elements. In: *Springer Handbook of Robotics*. Springer, pp. 243–282.

De Luca A and Flacco F (2011) A pd-type regulator with exact gravity cancellation for robots with flexible joints. In: *Robotics and Automation (ICRA), 2011 IEEE International Conference on*. IEEE, pp. 317–323.

De Luca A, Flacco F, Bicchi A and Schiavi R (2009) Nonlinear decoupled motion-stiffness control and collision detection/reaction for the vsa-ii variable stiffness device. In: *Intelligent Robots and Systems, 2009. IROS 2009. IEEE/RSJ International Conference on*. IEEE, pp. 5487–5494.

Della Santina C, Bianchi M, Grioli G, Angelini F, Catalano M, Garabini M and Bicchi A (2017a) Controlling soft robots: balancing feedback and feedforward elements. *IEEE Robotics & Automation Magazine* 24(3): 75–83.

Della Santina C, Catalano MG and Bicchi A (2020) *Soft Robots*. Berlin, Heidelberg: Springer Berlin Heidelberg. In Press (https://tinyurl.com/tbdw3g6).

Della Santina C, Piazza C, Gasparri GM, Bonilla M, Catalano MG, Grioli G, Garabini M and Bicchi A (2017b) The quest for natural machine motion: An open platform to fast-prototyping articulated soft robots. *IEEE Robotics & Automation Magazine* 24(1): 48–56.

Della Santina C and Rus D (2019) Control oriented modeling of soft robots: the polynomial curvature case. *IEEE Robotics and Automation Letters* 5(2): 290–298.

Flacco F and De Luca A (2011) Residual-based stiffness estimation in robots with flexible transmissions. In: *Robotics and Automation (ICRA), 2011 IEEE International Conference on*. IEEE, pp. 5541–5547.

Flacco F and De Luca A (2014) A pure signal-based stiffness estimation for vsa devices. In: *Robotics and Automation (ICRA), 2014 IEEE International Conference on*. IEEE, pp. 2418–2423. DOI:10.1109/icra.2014.6907195.

Hogan N (1985) Impedance control: An approach to manipulation: Part iiimplementation. *Journal of dynamic systems, measurement, and control* 107(1): 8–16.

Jafari A, Tsagarakis NG and Caldwell DG (2013) A novel intrinsically energy efficient actuator with adjustable stiffness (awas). *IEEE/ASME transactions on mechatronics* 18(1): 355–365.

Keppler M, Lakatos D, Ott C and Albu-Schäffer A (2018) Elastic structure preserving (esp) control for compliantly actuated robots. *IEEE Transactions on Robotics* 34(2): 317–335.

Mengacci R, Angelini F, Catalano MG, Grioli G, Bicchi A and Garabini M (2019) Stiffness bounds for resilient and stable physical interaction of articulated soft robots. *IEEE Robotics and Automation Letters* .

Ouyang P, Petz B and Xi F (2011) Iterative learning control with switching gain feedback for nonlinear systems. *Journal of Computational and Nonlinear Dynamics* 6(1): 011020.

Papadopoulos EG and Chasparis GC (2004) Analysis and model-based control of servomechanisms with friction. *Journal of dynamic systems, measurement, and control* 126(4): 911–915.

Petit F, Daasch A and Albu-Schäffer A (2015) Backstepping control of variable stiffness robots. *IEEE Transactions on Control*

[††] www.naturalmachinemotioninitiative.com

Systems Technology 23(6): 2195–2202. DOI:10.1109/tcst.2015.2404894.

Pratt GA and Williamson MM (1995) Series elastic actuators. In: *Intelligent Robots and Systems 95.'Human Robot Interaction and Cooperative Robots', Proceedings. 1995 IEEE/RSJ International Conference on*, volume 1. IEEE, pp. 399–406.

Siciliano B, Sciavicco L, Villani L and Oriolo G (2010) *Robotics: modelling, planning and control*, chapter 8.3. Springer Science & Business Media, pp. 309–319.

Spong MW (1998) Underactuated mechanical systems. In: *Control problems in robotics and automation*. Springer, pp. 135–150.

Tedrake R (2009) Underactuated robotics: Learning, planning, and control for efficient and agile machines course notes for mit 6.832. *Working draft edition* : 3.

Tomei P (1991) A simple pd controller for robots with elastic joints. *IEEE Transactions on automatic control* 36(10): 1208–1213.

Tonietti G, Schiavi R and Bicchi A (2005) Design and control of a variable stiffness actuator for safe and fast physical human/robot interaction. In: *Robotics and Automation, 2005. ICRA 2005. Proceedings of the 2005 IEEE International Conference on*. IEEE, pp. 526–531.

Tsagarakis NG, Laffranchi M, Vanderborght B and Caldwell DG (2009) A compact soft actuator unit for small scale human friendly robots. In: *Robotics and Automation, 2009. ICRA'09. IEEE International Conference on*. IEEE, pp. 4356–4362.

Vanderborght B, Albu-Schäffer A, Bicchi A, Burdet E, Caldwell DG, Carloni R, Catalano M, Eiberger O, Friedl W, Ganesh G et al. (2013) Variable impedance actuators: A review. *Robotics and autonomous systems* 61(12): 1601–1614.

Vanderborght B, Verrelst B, Van Ham R, Van Damme M, Lefeber D, Duran BMY and Beyl P (2006) Exploiting natural dynamics to reduce energy consumption by controlling the compliance of soft actuators. *The International Journal of Robotics Research* 25(4): 343–358.

Visser LC, Carloni R and Stramigioli S (2011) Energy-efficient variable stiffness actuators. *IEEE Transactions on Robotics* 27(5): 865–875.

Wang Y and Longman RW (1994) Limit cycle behavior and convergence to zero error in learning control with stick-slip friction. In: *Systems, Man, and Cybernetics, 1994. Humans, Information and Technology., 1994 IEEE International Conference on*, volume 3. IEEE, pp. 2774–2779.

Yu YQ, Li Q and Xu QP (2018) Pseudo-rigid-body dynamic modeling and analysis of compliant mechanisms. *Proceedings of the Institution of Mechanical Engineers, Part C: Journal of Mechanical Engineering Science* 232(9): 1665–1678.

Zhang J, Cheah CC and Collins SH (2017) Torque control in legged locomotion. In: *Bioinspired Legged Locomotion*. Elsevier, pp. 347–400.